AUGMENTING THE HEAT TRANSFER PERFORMANCE OF ROTATING TWO-PHASE THERMOSYPHONS

Carl Edward Schafer

NAVAL POSTGRADUATE SCHOOL
Monterey, California

THESIS

AUGMENTING THE HEAT TRANSFER PERFORMANCE OF ROTATING TWO-PHASE THERMOSYPHONS

by

Carl Edward Schafer, II

Thesis Advisor: P. J. Marto

December 1972

Approved for public release; distribution unlimited.

Augmenting the Heat Transfer Performance of Rotating Two-Phase Thermosyphons

by

Carl Edward Schafer, II
Lieutenant Commander, United States Navy
B.S., United States Naval Academy, 1963

Submitted in partial fulfillment of the requirements for the degree of

MASTER OF SCIENCE IN MECHANICAL ENGINEERING

and

MECHANICAL ENGINEER

from the

NAVAL POSTGRADUATE SCHOOL
December 1972

ABSTRACT

A Nusselt-type analysis was performed for laminar film condensation on the inside of a truncated rotating cone. Studies of this model revealed that the heat transfer capacity of the rotating thermosyphon was controlled by three thermal resistances; the condensate film thickness, condenser wall resistance, and the external heat transfer coefficient. A parametric study of the solution was performed for various values of these resistances and methods for reducing them were investigated.

A stainless steel thermosyphon was tested using various working fluids. A copper thermosyphon was constructed and tested using water. Different power levels and speeds of rotation were investigated. Efforts were made to increase the external heat transfer coefficient by regulation of the cooling spray.

Longitudinal grooving was studied as a means of reducing the heat transfer resistance of the internal condenser surface. An analytical model was developed for a triangular groove profile and a parametric analysis performed to show effects on heat transfer capabilities.

TABLE OF CONTENTS

TABLE OF SYMBOLS

A	surface area of condenser without external fins, ft^2
A_T	total surface area of externally finned condenser, ft^2
b	height of triangular grooves, ft
c_p	specific heat, Btu/lb_m - °F
f	friction factor, dimensionless
h	external heat transfer coefficient, $Btu/hr\text{-}ft^2\text{-}°F$
h_{eff}	effective external heat transfer coefficient for externally finned condenser, $Btu/hr\text{-}ft^2$ - °F
h_o	experimentally determined external heat transfer coefficient, $Btu/hr\text{-}ft^2\text{-}°F$
h_{fg}	latent heat of evaporation, Btu/lbm
k_f	thermal conductivity of the liquid, Btu/hr-ft-°F
k_w	thermal conductivity of condenser wall, Btu/hr-ft-°F
L_c	length of condenser, ft
$\dot{m}$	mass flow rate of coolant, lbm/hr
$\dot{M}_1$	mass flow rate of vapor condensing on fin, lbm/hr
$\dot{M}_2$	mass flow rate of vapor condensing in trough, lbm/hr
$\dot{M}_{total}$	total mass flow rate of condensate, lbm/hr
P_v	pressure of the vapor, lbf/ft^2
Q	theoretical heat transfer rate out of heat pipe, Btu/hr
Q_1	heat transfer through fin, Btu/hr
Q_2	heat transferred through trough, Btu/hr
Q_ℓ	no load heat generation, Btu/hr
R	internal condenser radius, ft
R_o	minimum internal radius of condenser, ft

R_2	minimum value of average starting radius for internally grooved condenser, ft
T_s	vapor saturation temperature, °F
T_{wall}	temperature of fin at fin-fluid interface, °F
T	inlet coolant temperature, °F
t	condenser wall thickness, ft
t*	effective condenser wall thickness, ft
u	velocity of liquid in x direction, ft/sec
$\bar{u}$	average velocity of liquid in x direction, ft/sec
v	velocity of vapor, ft/sec
w	velocity of liquid in z direction, ft/sec
$\bar{w}$	average velocity of liquid in z direction, ft/sec
W_{cp}	uncertainty of specific heat, dimensionless
$W_{\dot{m}}$	uncertainty of coolant mass flow rate, dimensionless
$W_{\Delta T}$	uncertainty of coolant temperature difference, dimensionless
$W_{Q\ell}$	uncertainty of no load heat generation, dimensionless
x	coordinate measuring distance along condenser length
y	coordinate measuring distance vertically from fin surface
z	coordinate measuring distance along triangular fin
GREEK	
α	fin half angle, radians
β	temperature gradient of fin-fluid interface, °F/ft
δ	film thickness, ft
δ^*	film thickness in trough, ft
ϵ	local trough width, ft
ϵ_o	minimum width of trough, ft

ϕ	half cone angle, radians
η_t	overall efficiency of externally finned condenser, dimensionless
ρ_f	density of the liquid, lbm/ft^3
ρ_v	density of the vapor, lbm/ft^3
σ	surface tension of the liquid, lbf/ft
τ	shear stress, lbf/ft^2
μ_f	viscosity of the liquid, lbm/ft-sec
μ_v	viscosity of the vapor, lbm/ft-sec
ω	angular velocity, rad/sec

I. INTRODUCTION

A. THE ROTATING TWO-PHASE THERMOSYPHON

The rotating two-phase closed thermosyphon is a device capable of transferring large quantities of heat from one place to another at nearly isothermal conditions. The three main parts of the thermosyphon are the evaporator, condenser, and the working fluid (Figure 1).

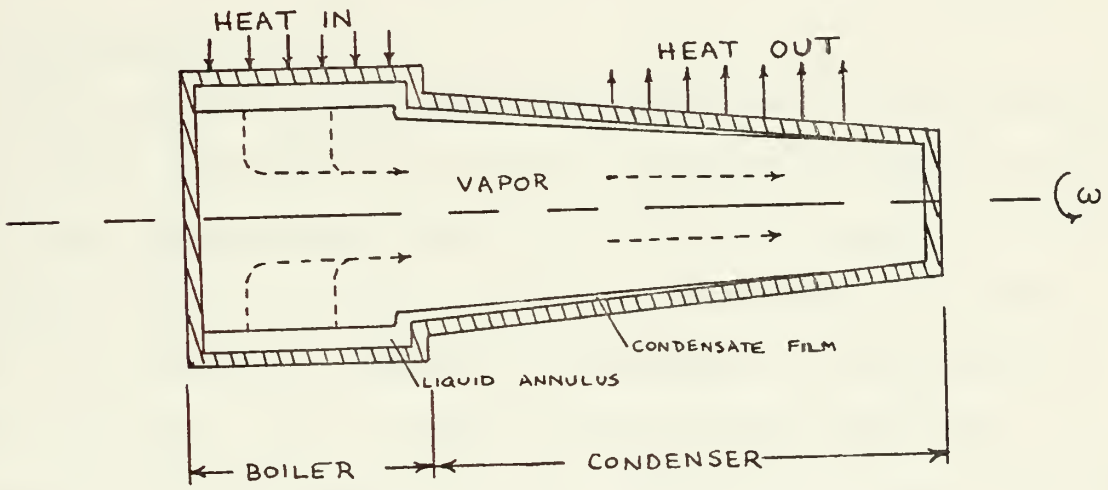

Fig. 1 Schematic Drawing of Typical Rotating Two-Phase Thermosyphon

Working fluid is evaporated in the evaporator. A small pressure gradient forces the vapor to flow towards the condenser where the latent heat of the vapor is removed upon condensation. The condenser wall has a small degree of taper opening towards the evaporator. A high centrifugal force created by rotation of the thermosyphon assembly about its longitudinal axis then drives the condensate back to the evaporator. It is this external force field for returning

the condensate that distinguishes the thermosyphon from a heat pipe. A heat pipe employs wicking material to provide the necessary driving force for the condensed working fluid. The thermosyphon may be stationary and depend on earth gravity to provide this driving force or it may be in motion and rely upon accelerations (centrifugal or otherwise) for the force. Because there is no wick in the thermosyphon and therefore, no large wick flow resistance, the thermosyphon can transfer large quantities of heat [1, 2].

B. BACKGROUND

Ballback initially studied the operational principles and performance characteristics of the rotating thermosyphon [3]. His analytic development was a Nusselt-type analysis for film condensation on the inside surface of a rotating truncated cone. He obtained a closed form solution for condensate film thickness, δ, by incorporation of the following assumptions in his analysis: (1) the rate of change of film thickness along the x-axis of the condenser (Figure 2) was much less than the tangent of the half cone angle, $\frac{d\delta}{dx} \ll \tan\phi$, (2) there were no shear stresses between the vapor and condensate, and (3) there was no thermal resistance in the condenser wall.

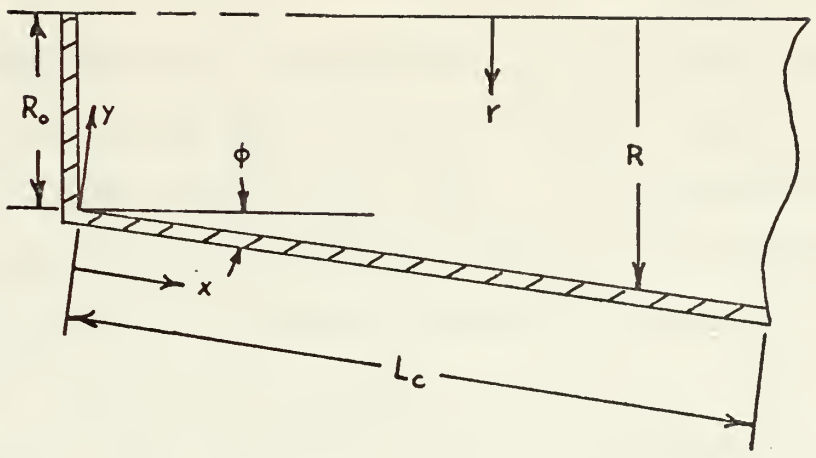

Figure 2 Coordinate System and Geometry for Condensate Film Analysis

Daley [4] performed a subsequent analysis which included the slope of the film thickness and thermal resistances due to the consenser wall and outside cooling mechanism. A second order differential equation for the condensate film thickness resulted. This equation's non-linearity proved to be very sensitive to the initial value of film thickness and consequently, no solutions were obtained for half-cone angles greater than zero. Newton's study [5] improved the analysis by including interfacial shear stress between vapor and condensate and accounting for change of vapor pressure along the condenser length. The problem was reduced to two simultaneous first order ordinary differential equations having as unknowns the condensate film thickness, $\delta(x)$, and the vapor velocity, $v(x)$. A Runge-Kutta numerical integration scheme was used to solve these equations on an IBM digital computer. The integration was started by assuming initial conditions,

$\delta = \delta_i$, $v = 0$, and $\frac{d\delta}{dx} = \tan\phi$ at $x = 0$. Results were obtained for half-cone angles of 0°, 0.1°, 0.2°, and 0.3°. This solution showed $\frac{d\delta}{dx} \ll \tan\phi$ and allowed simplification of the governing equation for $\delta(x)$. The approximate solution deviated from the numerical solution by a conservative 2.5% and agreement improved as the half cone angle was increased. For half cone angles greater than 0.3°, the approximation gave solutions that were independent of reasonably small values of initial film thickness, δ_i. Woodard [6] followed this development with a parametric study of the thermosyphon operating characteristics using the approximate solution of Newton.

Daley's study concluded the design and assembly of the thermosyphon. Newton operated the apparatus and was able to make the first comparisons between analytical and experimental results. Experimental data was 20% higher than maximum theory due to uncertainty of parameter measurements and existence of dropwise vice film condensation. Woodard was able to improve the instrumentation and implement thermosyphon cleaning procedures that promoted film condensation. He then obtained additional data for comparison with theory and also found that the condenser wall temperature was not constant along its length.

C. THESIS OBJECTIVES

The objectives of this study were to: (1) investigate the previous analytical solution in an attempt to improve thermosyphon performance, (2) improve instrumentation in

order to achieve more reliable experimental data, (3) obtain experimental results from different test sections for comparison with theory, (4) develop a theoretical model for a grooved condensing surface aimed at increasing the rate of heat transfer, and (5) conduct a parametric study of the grooved versus smooth condensing surfaces.

II. THEORETICAL PROGRAM

A. REVIEW

To improve the Nusselt-type analysis performed by Ballback and Daley, Newton included the effects of interfacial shear stress between liquid and vapor, and vapor pressure change along the condenser axis. Momentum, continuity, and energy equations were developed for an infinite simal condensate element. Momentum and continuity equations were also developed for one-dimensional, turbulent, and isothermal vapor flow. Reduction of these equations in Newton's study [5] resulted in two simultaneous first order ordinary differential equations

$$\frac{dv}{dx} = \frac{2(R_o + x\sin\phi)(T_s - T_\infty)}{\rho_v\left[\frac{\delta}{k_f} + \frac{t}{k_w} + \frac{1}{h}\right]R^2 h_{fg}} - \frac{2v}{R}\left[\sin\phi - \cos\phi\,\frac{d\delta}{dx}\right] \quad (1)$$

$$\frac{d\delta}{dx} = \tan\phi - \frac{\rho_v v^2 f\left[\frac{P_1}{R} + \frac{P_2}{2}\right] + \rho_v v\left[\frac{\mu_f R^2}{2\rho_f} - 2P_1\frac{dv}{dx}\right]}{P_1\cos\phi\left[\rho_f\omega^2 R + \frac{2\rho_v v^2}{R}\right]} \quad (2)$$

$$P_1 = (R_o + x\sin\phi)\frac{\delta^3}{3} - \cos\phi\,\frac{5}{24}\,\delta^4$$

$$P_2 = (R_o + x\sin\phi)\frac{\delta^2}{2} - \cos\phi\,\frac{\delta^3}{3}$$

with the following initial conditions:

$$\delta(0) = \delta_i$$

$$v(0) = 0$$

A Runge Kutta numerical integration scheme was used to solve these equations on an IBM digital computer. Solutions were highly dependent upon the choice of initial film thickness and because of instability problems, were only obtainable for half cone angles of 0°, 0.1°, 0.2°, and 0.3°. The results indicated that, except near the ends of the condenser, $\frac{d\delta}{dx} \ll \tan\phi$. This approximation and an order of magnitude analysis applied to equations (1) and (2) reduced them to a first order differential equation in $v(x)$ and a cubic equation for $\delta(x)$

$$\frac{dv}{dx} = \frac{2(R_o + x\sin\phi)(T_s - T_\infty)}{\rho_v\left[\frac{\delta}{k_f} + \frac{t}{k_w} + \frac{1}{h}\right]R^2 h_{fg}} - \frac{2v\sin\phi}{R} \qquad (3)$$

$$\frac{\delta^3}{3} R\sin\phi\left[\rho_f\omega^2 R + \frac{2\rho_v v^2}{R}\right] - \rho_v v^2 f\left[R\frac{\delta^2}{4}\right] - \rho_v v\frac{\mu_f R^2}{2\rho_f} = 0 \qquad (4)$$

Equation (3) with the use of equation (4) was numerically integrated over the length of the condenser using initial values of zero film thickness and zero velocity. Having found vapor velocity at a particular step, a subroutine was used to solve equation (4). This resulting value of film thickness was used to find $v(x)$ for the next step of the integration. The total heat transfer rate was then obtained by summing the heat contribution of each incremented step over the condenser length

$$\Delta Q = \frac{2\pi(R_o + x\sin\phi)(T_s - T_\infty)\,\Delta x}{\frac{\delta(x)}{k_f} + \frac{t}{k_w} + \frac{1}{h}} \qquad (5)$$

Results from equations (3) and (4) were 2.5% lower than the more exact solution (from equations (1) and (2)) for half cone angles of 0.3° and less. For larger half cone angles (up to 3.0°) the approximation gave results that were independent of the small initial film thickness. Thus, equations (3), (4), and (5) were used to obtain theoretical results for condensate film thickness and heat transfer from the thermosyphon.

B. MODIFICATIONS TO THERMOSYPHON THEORETICAL RESULTS

Woodard's experimental data indicated that modifications to the computerized solution of equations (3) and (4) were necessary. The outside condenser wall temperature had originally been taken as constant over its entire length. This value was the average of three or four surface thermocouples which were placed at different locations along the condenser. The thermocouple closest to the evaporator usually indicated a higher temperature than the remaining thermocouples. Relocation and addition of thermocouples in subsequent runs established the existence of a steep temperature gradient on the condenser exterior near the evaporator. Equations (3), (4), and (5) and the computer solution were then modified to account for this variation in wall temperature. Equations (6), (7), and (8) reflect these changes.

$$\frac{dv}{dx} = \frac{2(R_o + x \sin\phi)(T_s - T_{w(x)})}{\rho_v \left[\frac{\delta(x)}{k_f} + \frac{t}{k_w}\right] R^2 h_{fg}} - \frac{2 v \sin\phi}{R} \qquad (6)$$

$$\frac{\delta^3}{3} R \sin\phi \left[\rho_f \omega^2 R + \frac{2\rho_v v^2}{R}\right] - \rho_v v^2 f \left[R \frac{\delta^2}{4}\right] - \rho_v v \frac{\mu_f R^2}{2\rho_f} = 0 \quad (7)$$

$$\Delta Q = \frac{2\pi (R_o + x \sin\phi)(T_s - T_{w(x)}) \Delta x}{\frac{\delta(x)}{k_f} + \frac{t}{k_w}} \quad (8)$$

Since varying temperatures were encountered not only from one data point to another but also along the length of the condenser as described above, the change in fluid, vapor, and wall properties with temperature had to be accounted for. A least-squares polynomial was generated for the various properties over the temperature ranges involved. These polynomials were placed in the computer solution such that new properties were computed at each incremental length.

The last modifications made to the computer solution involved the friction factor used to account for shear forces at the vapor-condensate interface. A Reynolds number for the vapor flow was calculated at each incremental condenser length. Engineering judgment indicated that turbulence in the vapor flow would occur at approximately the same critical Reynolds number as pipe flow. Accordingly, the computer solution was changed to use laminar or turbulent flow friction factors when the vapor flow Reynolds number was above or below a critical value of 2300. This effect was found to be small as evidenced by results obtained using a friction factor ten times that normally encountered.

C. PARAMETRIC STUDY OF SMOOTH CONDENSER

Woodard's thesis [6] included a parametric study for the thermosyphon with a smooth stainless steel interior surface. The variables considered were condenser geometry, rotational speed, working fluids and the exterior heat transfer coefficient. In an attempt to improve the heat transfer capabilities of the thermosyphon, it became necessary to determine those factors which limited performance. Representative values of condensate thickness and average external heat transfer coefficient taken from Woodard's experimental results gave the following thermal resistances:

THERMAL RESISTANCE		REPRESENTATIVE VALUES	
INSIDE FILM	$\frac{\delta}{k_f}$	$\delta \approx .00035$ (ft) $k_f \approx .35$ (Btu/hr-ft-°F)	$\frac{\delta}{k_f} \approx .001$
WALL	$\frac{t}{k_w}$	$t \approx .0052$ (ft) $k_w \approx 9.0$ (Btu/hr-ft-°F)	$\frac{t}{k_w} \approx .0006$
OUTSIDE HEAT TRANSFER COEFFICIENT	$\frac{1}{h}$	$1200 < h_o < 1600$ (Btu/hr-ft²-°F)	$\frac{1}{h} \approx .0009$

Table 1 Thermosyphon Thermal Resistances from Data of Woodard [6]

Table 1 clearly indicates the relative importance of each thermal resistance and shows those factors having strongest influence on overall heat transfer capabilities. The external heat transfer coefficient, h, was found to vary from 1200 to 1600 Btu/hr-ft^2-°F and thus rival the condensate film thickness (about .00035 ft) for dominance.

1. Wall Resistance

Although not the controlling factor, wall resistance is the easiest to reduce. A copper test section, for example, would reduce this resistance by a factor of 25. Of note, however, is the fact that copper represents the material possessing the highest thermal conductivity other than silver and is therefore a limiting value. Reduction of wall thickness becomes impractical beyond certain strength limitations or when internal grooving of the condenser is considered.

2. Internal Resistance

Of ordinary fluids, water possesses the highest latent heat of vaporization and thermal conductivity. This choice of working fluid limits reduction of the film resistance to some means of reducing the condensate film thickness. Longitudinal grooving of the interior condenser surface as discussed later would be an effective way of doing this.

3. External Resistance

Lowering of the external thermal resistance involves an increase in the external surface area and/or an increase in the heat transfer coefficient. These appear to be the most difficult modifications to implement. The addition of small annular fins to the exterior surface does increase the cooling surface area but also complicates the temperature distribution in the condenser wall (an effect that is likewise experienced with internal grooving). Thermocouple location and the positioning of coolant spray nozzles becomes more difficult.

As a means of comparison, external annular fins of copper having a width of 1/16 inch, separation of 1/16 inch and protruding from the surface by 3/16 of an inch were chosen. Using Holman [7], a fin efficiency of about 0.80 and overall efficiency of 0.82 were obtained. The overall efficiency and ratio of areas (total finned and surface area to the surface area without fins) were then used to obtain an effective value of heat transfer coefficient to use in the computerized model according to the formula [8]

$$h_{eff} = h_o \eta_t \frac{A_T}{A} \tag{9}$$

where h_o = 1500 Btu/hr-ft^2-°F

This effective coefficient was about 5000 Btu/hr-ft^2-°F, or over three times the experimentally obtained value for existing condensers. It was then used in the analytical model to represent the thermosyphon improvement for addition of external fins.

Other methods for improving heat transfer coefficient include changes in coolant spray nozzle size, location, quantity, and the coolant flow rate. This would affect the droplet size, distribution, and velocity. Lack of a suitable increase in the heat transfer coefficient by any of the above methods would then necessitate a thorough study aimed at determining the maximum possible coefficient and then design of a cooling system that could approach this value. Such a possibility might be construction of a coolant jacket that would rotate synchronously with the thermosyphon. The coolant

would have solid body rotation with the thermosyphon while axial flow would provide the desired convection cooling.

4. Analysis

Figures 3 , 4 , and 5 depict the results of changing the three possible thermal resistances. All graphs are plotted with saturation temperature of the working fluid on the abscissa and the heat transfer rate of the thermosyphon on the ordinate. With the parameters h, ϕ, and RPM held constant, such a graph represents thermosyphon reponse as a function of fluid properties. Variance of an individual parameter then produces a family of curves for each figure and thereby illustrates the effect of that parameter on the response of the thermosyphon. For the study, values of external heat transfer coefficient used were 1000, 1500, and 5000 Btu/hr-ft^2-°F. Thermosyphon rotational speeds of 1000 and 3000 RPM were used. Two condenser materials, copper and stainless steel, were compared as well as an external fin arrangement that would increase cooling surface area by 4 times. The condenser half cone angle of 1° and working fluid of water were unchanged throughout the study.

D. THEORY FOR INTERNALLY GROOVED CONDENSER

Longitudinal grooving of the inside condenser surface is one method of lowering the film thermal resistance. Gregorig [9] has shown that longitudinally grooved vertical condensing surfaces will have a net effective thermal resistance less than that of a smooth condensing surface. He showed that this effect was caused by a pressure gradient in the condensate

due to the surface tension forces of the liquid and the local radius of curvature. For the geometry of Figure 6, the pressure at point 1 and 2 are computed to be

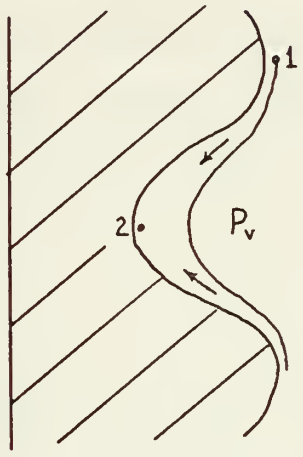

$$P_1 = P_v + \frac{2\sigma}{R_1}$$

$$P_2 = P_v - \frac{2\sigma}{R_2}$$

Figure 6. Grooved Condenser Wall

where the change in sign results from the change in sign of the curvature. Assuming vapor pressure, P_v , to be constant, P_1 is thus greater than P_2 and a driving force sends condensate to the bottom of the groove. Although heat transfer is poorer in the trough, very high heat transfer occurs near the crest resulting in an overall increase. When applied to the rotating thermosyphon, the impressed rotational gravity field would overshadow the surface tension induced force. Nevertheless, results would be similar with the thin film occurring at the crest of the grooves. An experimental study by Lustenader, Richter, and Neugebauer [10] has confirmed the existence of higher heat transfer rates for thin film condensation on a fluted surface.

For simplicity of analysis, a groove profile having a triangular cross section was chosen. An enlarged view of the triangular fin geometry is depicted in Figure 7 along with appropriate dimensions. The x-axis is normal to the y-z plane and is coincidental with the fin tip. The radius, r_1 , for a cross section is taken arbitrarily as halfway between tip and bottom of the groove and is represented by:

$$r_1 = R_2 + x \sin \phi \tag{10}$$

This choice of radius makes the centrifugal gravity force constant for the entire depth of groove at each x location. Condensate from the triangular fins collects in the trough of the groove which then acts as the primary path for return of the fluid to the evaporator. A greater film thickness in the trough allows very little heat transfer when compared to the thinner film existing on the exposed fins.

1. Assumptions

The theoretical model for internally grooved condenser was developed based on the following assumptions [3]:

a. Film condensation, not dropwise condensation, occurs in the condenser section.

b. The condensate film undergoes laminar flow.

c. Subcooling of the condensate may be neglected.

d. Momentum changes through the condensate are small and thus there is essentially a static balance of forces.

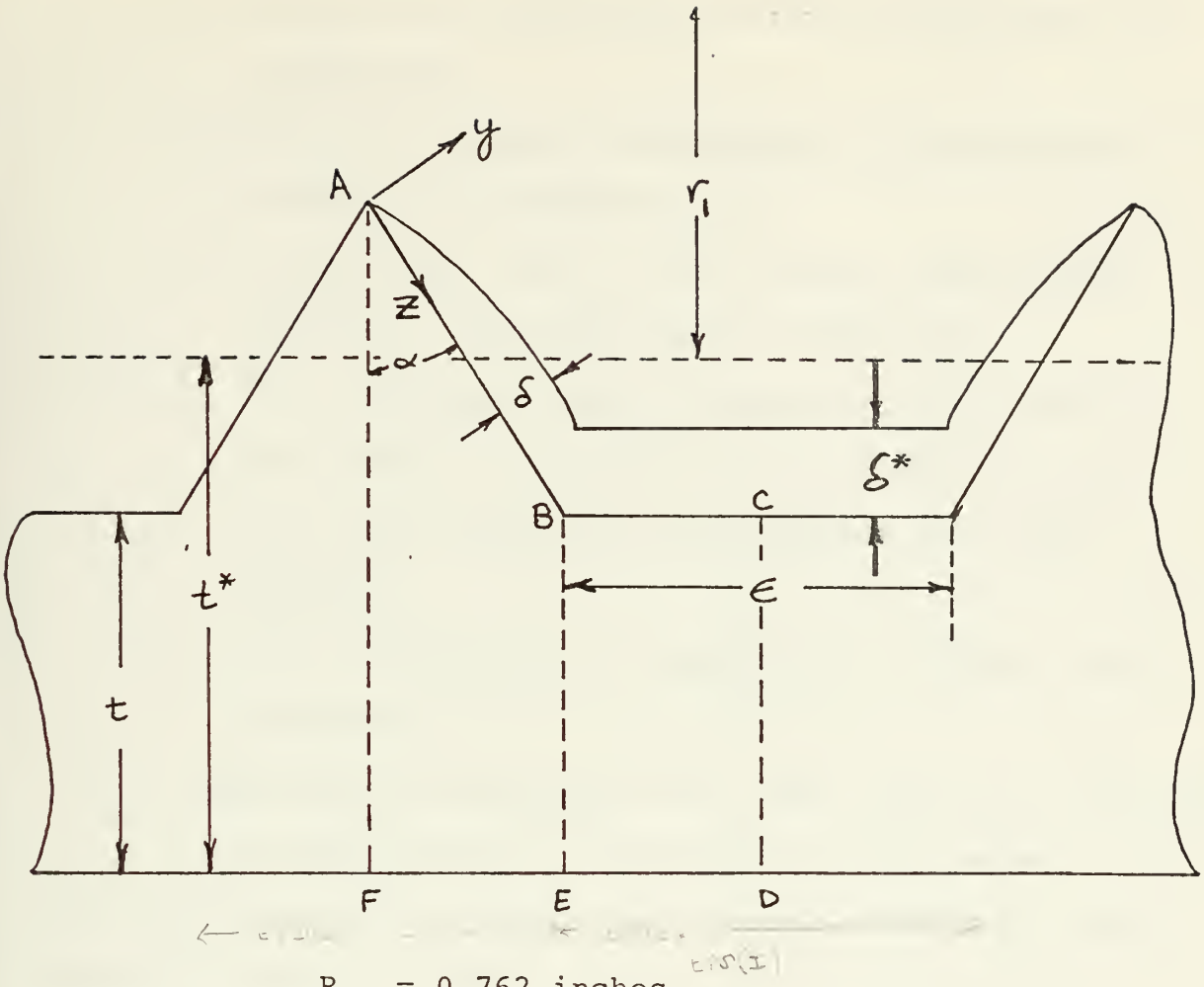

R_2 = 0.762 inches

t = 0.0375 inches

b = 0.025 inches

t* = 0.050 inches

Figure 7 Geometry and Coordinate System for Triangular Grooves

e. There is no interfacial shear between vapor and condensate.

f. There is a linear distribution of temperature through the condensate film.

g. Centrifugal force is much greater than earth gravity. The latter may be neglected.

h. The condensate film thickness is much less than the radius of curvature of the condenser wall.

i. The fluid density is much greater than vapor density.

j. The thermosyphon is operating at a steady state condition.

2. Mass Flow in Z-Direction (per unit length in x-direction)

In a manner similar to Ballback's force balance on an infinitessimal fluid element, the momentum equation in the z-direction may be written

$$\frac{\partial \tau_z}{\partial y} = \frac{\partial p}{\partial z} - \rho_f \omega^2 r_1 \cos\phi \cos\alpha \qquad (11)$$

where $\frac{dp}{dz}$ may be neglected. Integrating equation (11) from τ_z to 0 and y to δ gives

$$\tau_z = \rho_f \omega^2 r_1 \cos\phi \cos\alpha \, (\delta - y) \qquad (12)$$

$$\tau_z = \mu_f \frac{\partial w}{\partial y}$$

Integration of equation (12) from 0 to w and 0 to y gives an expression for the velocity of the fluid

$$w = \frac{\rho_f \omega^2 r_1 \cos\phi \cos\alpha}{\mu_f} \left(\delta y - \frac{y^2}{2}\right) \qquad (13)$$

which may be used to find an average velocity using the expression

$$\bar{w} = \frac{1}{\delta}\int_0^{\delta} w\, dy = \frac{\rho_f \omega^2 [R_2 + x \sin\phi] \cos\phi \cos\alpha\, \delta^2}{3\mu_f} \quad (14)$$

The mass flow rate at any z location on the fin may be written as

$$\dot{M}_1 = \rho_f \delta \bar{w} \quad (15)$$

Substitution of equation (14) into equation (15) then gives the mass flow rate as a function of film thickness

$$\dot{M}_1 = \frac{\rho_f^2 \omega^2 (R_2 + x \sin\phi) \cos\phi \cos\alpha\, \delta^3}{3\mu_f} \quad (16)$$

3. Mass Flow in X-Direction

An assumption is made that the mass flow rate in the x-direction along the fins is negligible compared to the axial flow in the troughs. The trough mass flow at any x location is therefore the total mass flow up to that point. Using the x-direction momentum equation for an infinitessimal fluid element in the trough

$$\frac{\partial \tau_x}{\partial y} = -\rho_f \omega^2 r_1 \sin\phi \quad (17)$$

and proceeding in a manner analogous to that for the z direction, an expression for average film velocity in the trough may be obtained

$$\bar{u} = \frac{1}{\delta^*}\int_0^{\delta^*} u\, dy = \frac{\rho_f \omega^2 (R_2 + x \sin\phi) \sin\phi\, \delta^{*2}}{3\mu_f} \quad (18)$$

The total mass rate of condensate flow in the longitudinal direction in terms of trough film thickness, δ^*, and x location becomes

$$\dot{M}_{TOTAL} = \rho_f \bar{u} A_{TROUGH} \tag{19}$$

$$\dot{M}_{TOTAL} = \frac{\rho_f^2 \omega^2 (R_2 + x \sin\phi) \sin\phi}{3\mu_f} \left(\epsilon \delta^{*3} + \delta^{*4} \cos\alpha \sin\alpha\right)$$

where A_{trough} = cross sectional area of trough

4. Energy Equation for Fin Condensate (per unit length in the x-direction).

An energy balance for a differential element of the fin condensate flowing in the z-direction yields the necessary relation between film thickness δ and distance along the fin, z.

$$dQ_1 = h_{fg}\, d\dot{M}_1 = \frac{k_f (T_s - T_{WALL})}{\delta} dz \tag{20}$$

The interface wall temperature, T_{wall}, is obviously a function of distance z. Since the film thickness at the apex of the fin (point A in Figure 7) is zero, it must be assumed that at the apex the temperature is the same as vapor saturation temperature. It may also be deduced that lines A-F and C-D represent insulated boundaries because of profile symmetry. An adequate estimate of the interior wall temperature at point C may be found by equating heat fluxes for an infinite simal area at this point

$$\frac{Q}{A} = \frac{(T_s - T_\infty)}{\frac{\delta^*}{k_f} + \frac{t}{k_w} + \frac{1}{h}} = \frac{(T_s - T_c)}{\frac{\delta^*}{k_f}} \qquad (21)$$

Thus, the wall temperature varies somehow from T_s to T_c along the wall from point A to C. Observing that thin films occur along the side of the fin when compared to the film thickness in the trough, it may be deduced that most of the heat flow occurs through the region of the fin. Also, when considering one-dimensional flow through section ABEF, this heat flow may be so great that its only limitation is the amount that can be removed externally from FE. With this limitation and the lower temperatures existing in section BCDE, it becomes apparent that a two-dimensional heat flow problem exists. Such two-dimensional heat flow in the condenser wall results in a wall-film interface temperature that may not be a linear function of z. Until a detailed two-dimensional analysis is performed, a linear relationship is assumed and the temperature difference in equation (20) becomes

$$T_{WALL} = T_s - \beta z$$
$$T_s - T_{WALL} = \beta z \qquad (22)$$

Equation (16) is used to find the differential, $d\dot{M}_1$, which with equation (22) is substituted into equation (20). Equation (20) is then integrated from 0 to δ and 0 to z to obtain an expression for film thickness, δ

$$\delta = \left[\frac{2 k_f \beta \mu_f}{\rho_f^2 \omega^2 (R_2 + x \sin\phi) h_{fg} \cos\alpha \cos\phi} \right]^{1/4} z^{1/2} \qquad (23).$$

5. Energy Equation for Trough Condensate

Even though the condensate in the trough has a larger thickness, there is a small amount of vapor condensation on its surface. The energy balance gives an expression for the mass rate entering the trough (per unit length in x direction) in this manner:

$$dQ_2 = h_{fg}\, d\dot{M}_2 = \frac{(T_s - T_\infty)\,\epsilon}{\frac{\delta^*}{k_f} + \frac{t}{k_w} + \frac{1}{h}}\, dx \qquad (24)$$

where ϵ = local width of trough

6. Determination of Heat Transfer Rate

Using the energy balance of equation (20) with the results of equations (16) and (23), the heat flow for a fin element of width dx and length z_o becomes

$$dQ_1 = h_{fg}\, d\dot{M}_1 = \frac{(2 k_f \beta)^{3/4} (\rho_f \omega)^{1/2} \left[(R_2 + x \sin\phi) h_{fg} \cos\alpha \cos\phi \right]^{1/4} z^{*\,3/2}}{3 (\mu_f)^{1/4}}\, dx \qquad (25)$$

where $z^* = z_o - \delta^* \cos\alpha$

The method used to obtain an approximation of the inside wall temperature gradient, β, was to equate heat flow through the fin (equation (25)) to that which could flow through an element having width EF and having an estimated equivalent height t* (equal to t plus one-half the groove height).

$$\frac{\left(T_s - T_\infty - \frac{\beta \ell}{2}\right)}{\frac{t^*}{k_w} + \frac{1}{h}} = \frac{\left(2 k_f \beta\right)^{3/4} \left(\rho_f \omega\right)^{1/2} \left[\left(R_2 + x \sin\phi\right) h_{fg} \cos\alpha \cos\phi\right]^{1/4} \Delta x \left(\bar{z}''\right)^{3/2}}{3 \left(\mu_f\right)^{1/4}} \tag{26}$$

This resulted in a transcendental equation for β which was then solved using an iterative scheme at each incremental length in the computerized analytical model of the grooved condenser.

The mass continuity equation for any x location of the condenser may be written as

$$\dot{M}_{total} = \int_0^x \frac{d\dot{M}_1}{dx}\, dx + \int_0^x \frac{d\dot{M}_2}{dx}\, dx \tag{27}$$

where $\frac{d\dot{M}_1}{dx}$ is obtained from equation (25), and

$\frac{d\dot{M}_2}{dx}$ is obtained from equation (24).

The first step in evaluating this integral is to divide the condenser into a large number of incremental elements of length ΔX. Equations (24) and (25) are then used to find the mass flow rate condensed in the first Δx element. This mass flow rate, added to any initial flow from the condenser

endpiece, may be used in equation (19) to solve for the trough film thickness, δ^*, of the first incremental length. The above value of δ^* is then used in equations (24) and (25) to find the mass rate condensed in the second incremental Δx element. The above process is repeated until the entire condenser length has been traversed. The heat transferred from the condenser may then be computed for each incremental element and summed over the length using equations (24) and (25) or obtained from the product of total condensate mass flow rate and the latent heat of vaporization of the working fluid.

E. PARAMETRIC STUDY OF INTERNALLY GROOVED CONDENSER

The theory developed for the internal grooving of the condenser section was intended to reduce the film thermal resistance and increase the overall heat transfer capability of the thermosyphon. As in the smooth condenser parametric analysis, the working fluid and half cone angle remained fixed. For the grooved geometry, the minimum trough width, ϵ_o, was arbitrarily chosen to have the same dimension as the base of a fin. Plots of heat transfer rate versus fluid saturation temperature were made as individual values of the parameters were changed. The external heat transfer coefficient was varied from 1000 to 5000 Btu/hr ft^2 °F to generate one family of curves. Thermosyphon speed of rotation was varied from 1000 to 3000 RPM to generate another family of curves. A comparison of these families of curves was then made for the condenser test sections involved, stainless

steel and copper. Also, as a final comparison, external fins of the type discussed in the smooth condenser study were added to each internally grooved test section.

F. DISCUSSION OF ANALYTICAL RESULTS

In actual operation, the heat transfer rate of the thermosyphon is determined by its application. An equilibrium saturation temperature at which the thermosyphon will operate is reached for all other operating conditions. Woodard's study [6] has already shown water to be the most satisfactory working fluid.

Figures 3-9 display the interrelationships of the previously discussed thermal resistances on thermosyphon performance. While an increasing rotational speed increases the heat transfer for any fixed external h, the percentage change becomes larger when other thermal resistances are lowered. Proportionate increases from 1.25 to 1.70 are obtainable upon comparison of Figures 3 and 4 . A similar increase for the internally grooved condenser is not experienced in Figures 6 and 7. This may be expected since offsetting effects in the theory make heat transfer for the grooved condenser essentially independent of rotational speed.

A basic explanation is that a higher rotational speed decreases the film thickness and causes an increase in the heat transfer rate. The smaller film thickness, however, increases the local wall temperature and causes a decrease in the heat transfer rate.

Similarly, a larger external heat transfer coefficient for a fixed rotational speed is seen to produce proportionately larger heat transfer rates as other thermal resistances are reduced. The ratios increase from 1.05 to 7.0 for the comparisons of Figures 3, 5, 6, and 8. Figure 9 represents the maximum possible increase in heat transfer under the given conditions by comparing the poorest curve of Figure 3 to the best curve of Figure 6. Of note is the fact that the best curve in Figure 9 exceeds the entrainment limit of the thermosyphon as discussed by Ballback [3]. Experimental data of Hewitt et al, can be used to predict the entrainment limit for the present case and places it some 10-20% below the condenser limit of an internally grooved, externally finned, copper test section [11]. Since the entrainment limit is dependent upon the square of the condenser diameter, a study could be performed to determine that diameter at which the condenser and entrainment limits are approximately equal.

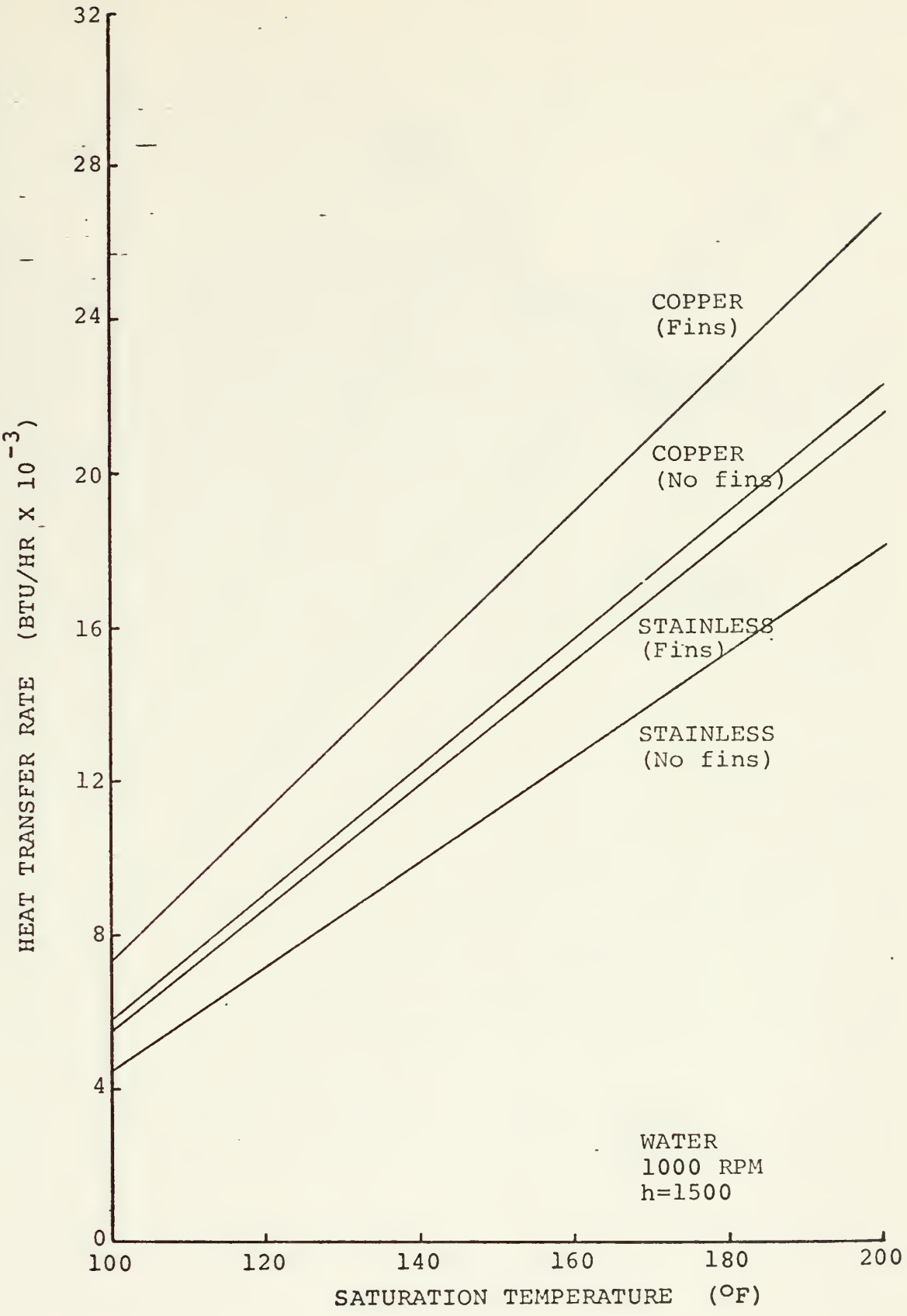

Figure 3 Heat Transfer Rate vs. Saturation Temperature for Internally Smooth Condenser

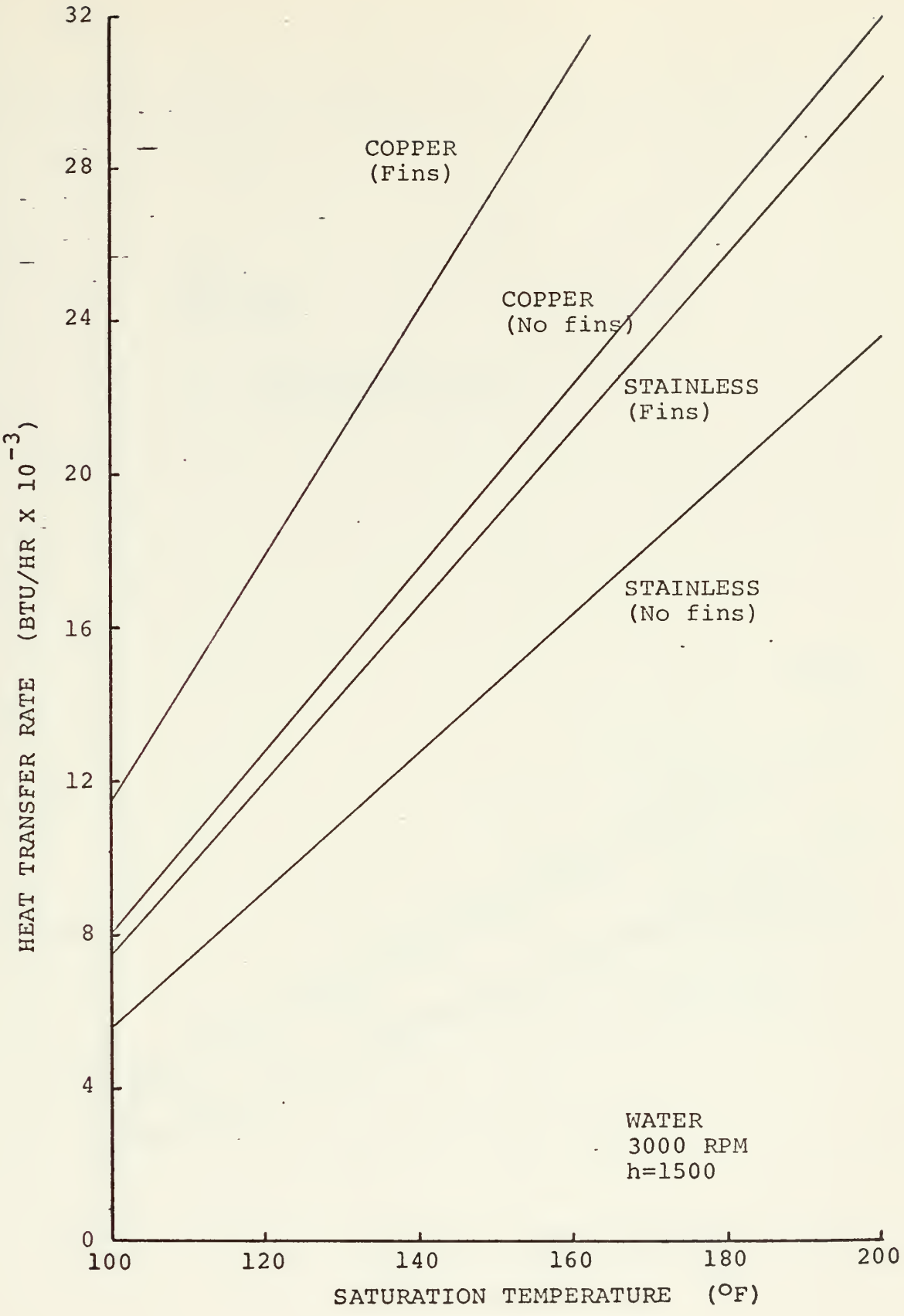

Figure 4 Heat Transfer Rate vs. Saturation Temperature for Internally Smooth Condenser

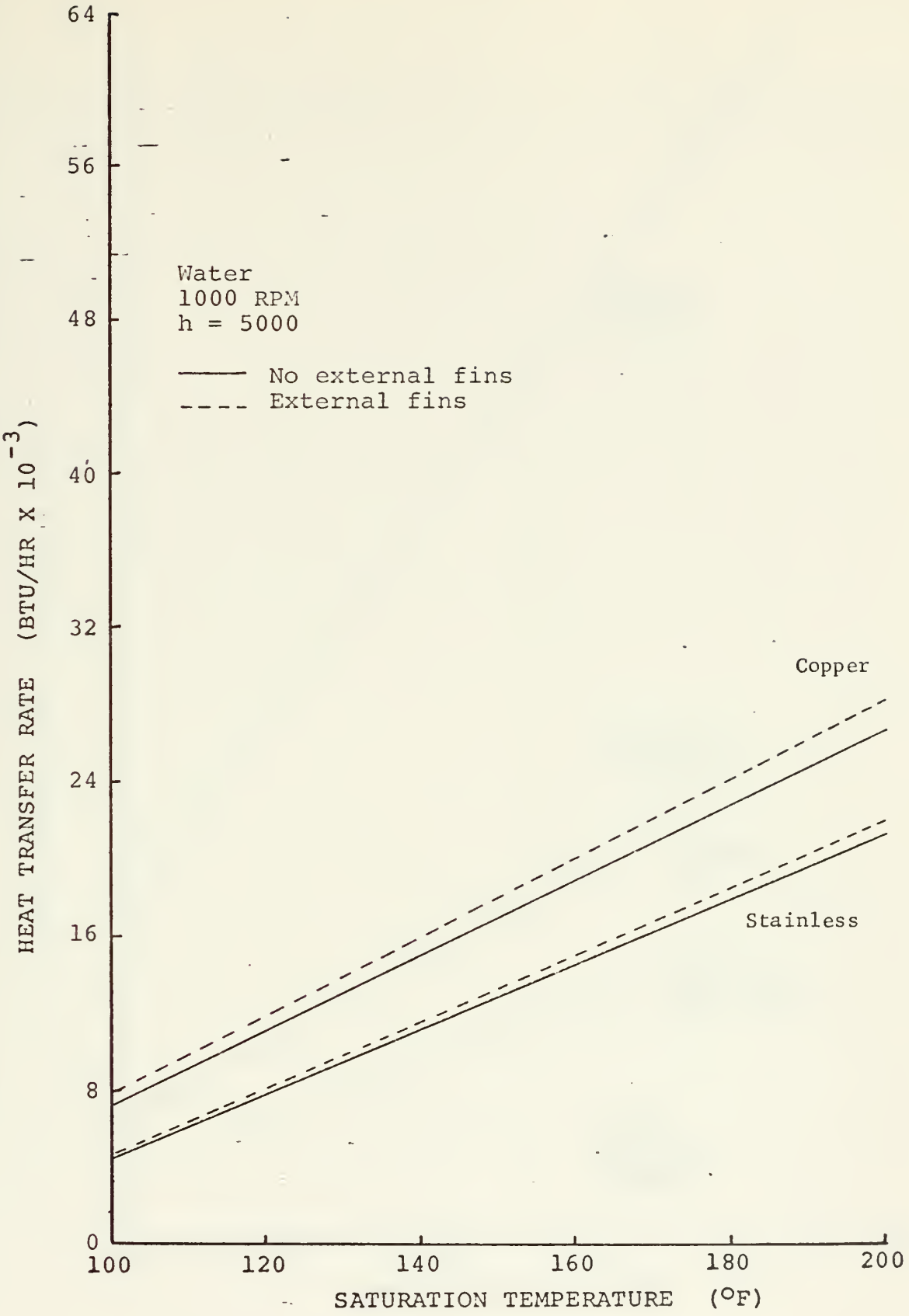

Figure 5 Heat Transfer Rate vs. Saturation Temperature for Internally Smooth Condenser

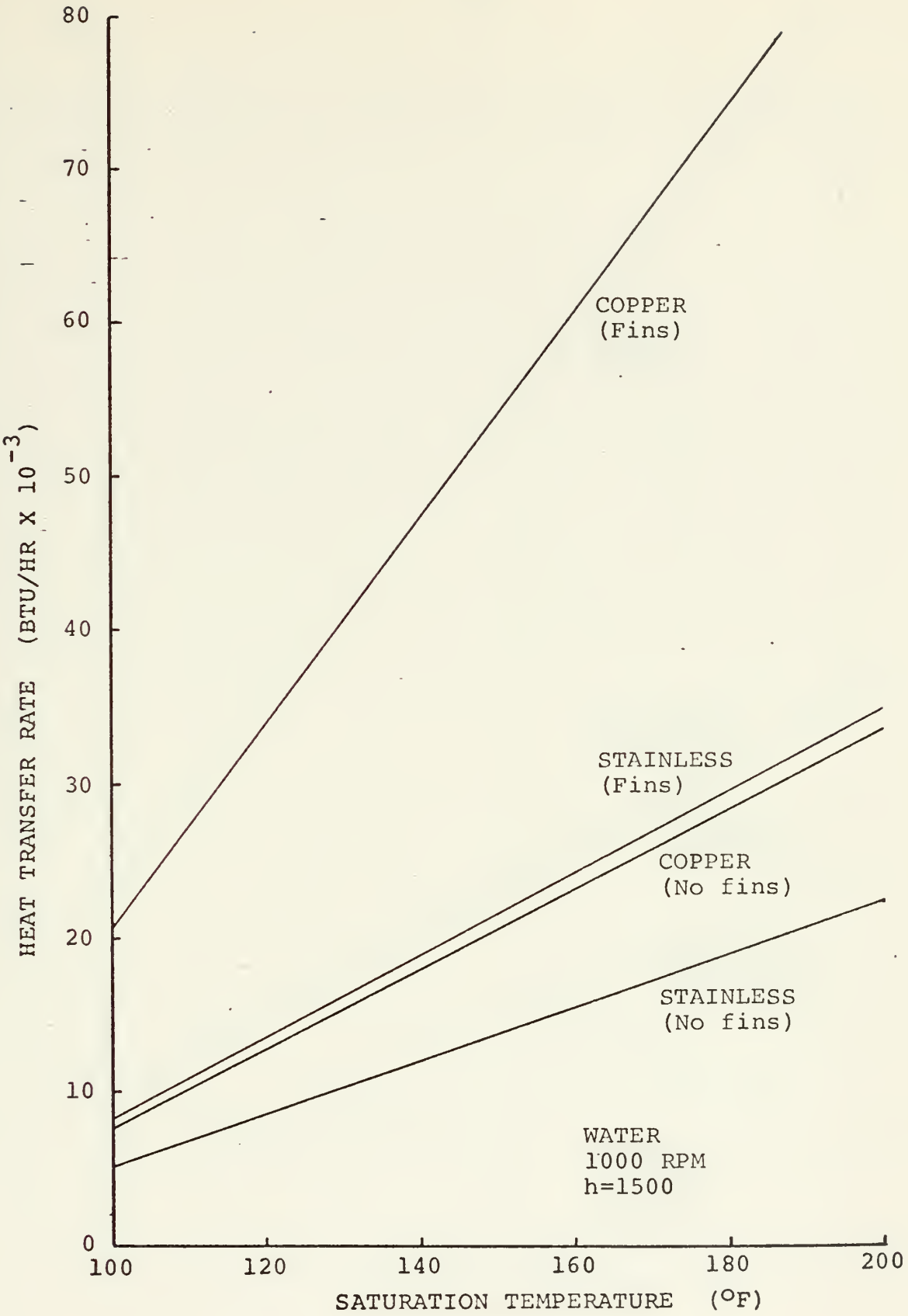

Figure 6 Heat Transfer Rate vs. Saturation Temperature for Internally Grooved Condenser

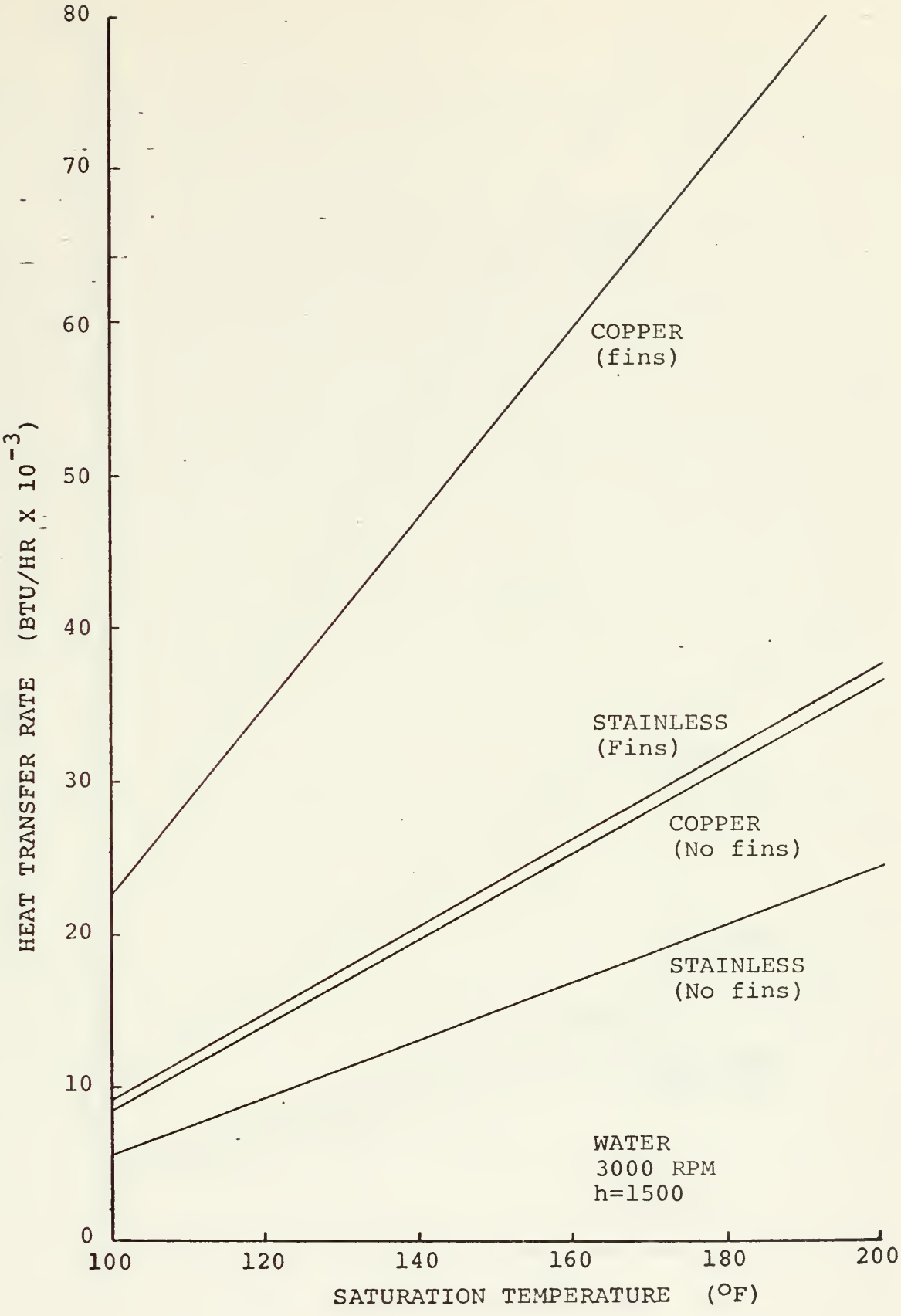

Figure 7 Heat Transfer Rate vs. Saturation Temperature for Internally Grooved Condenser

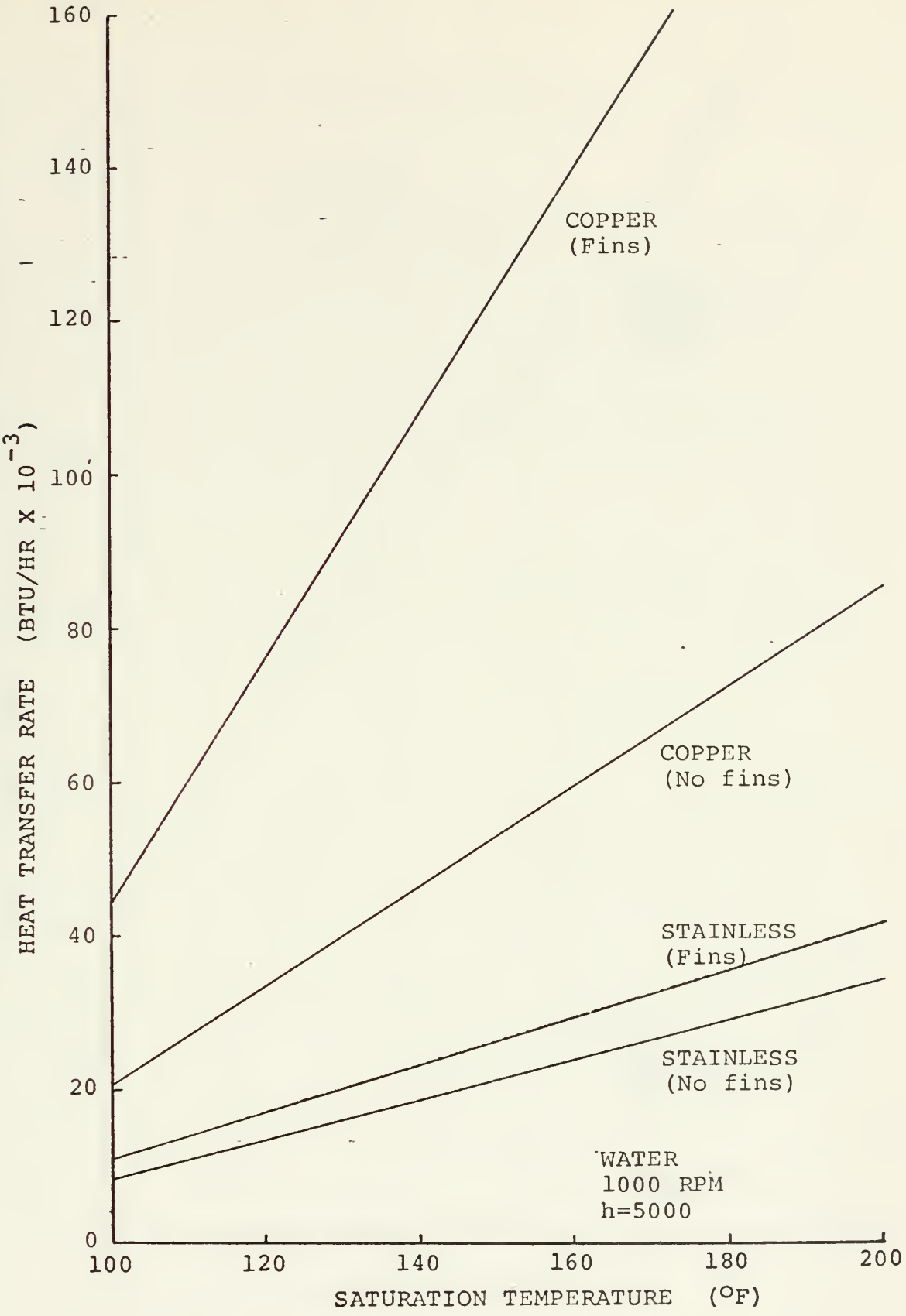

Figure 8 Heat Transfer Rate vs. Saturation Temperature for Internally Grooved Condenser

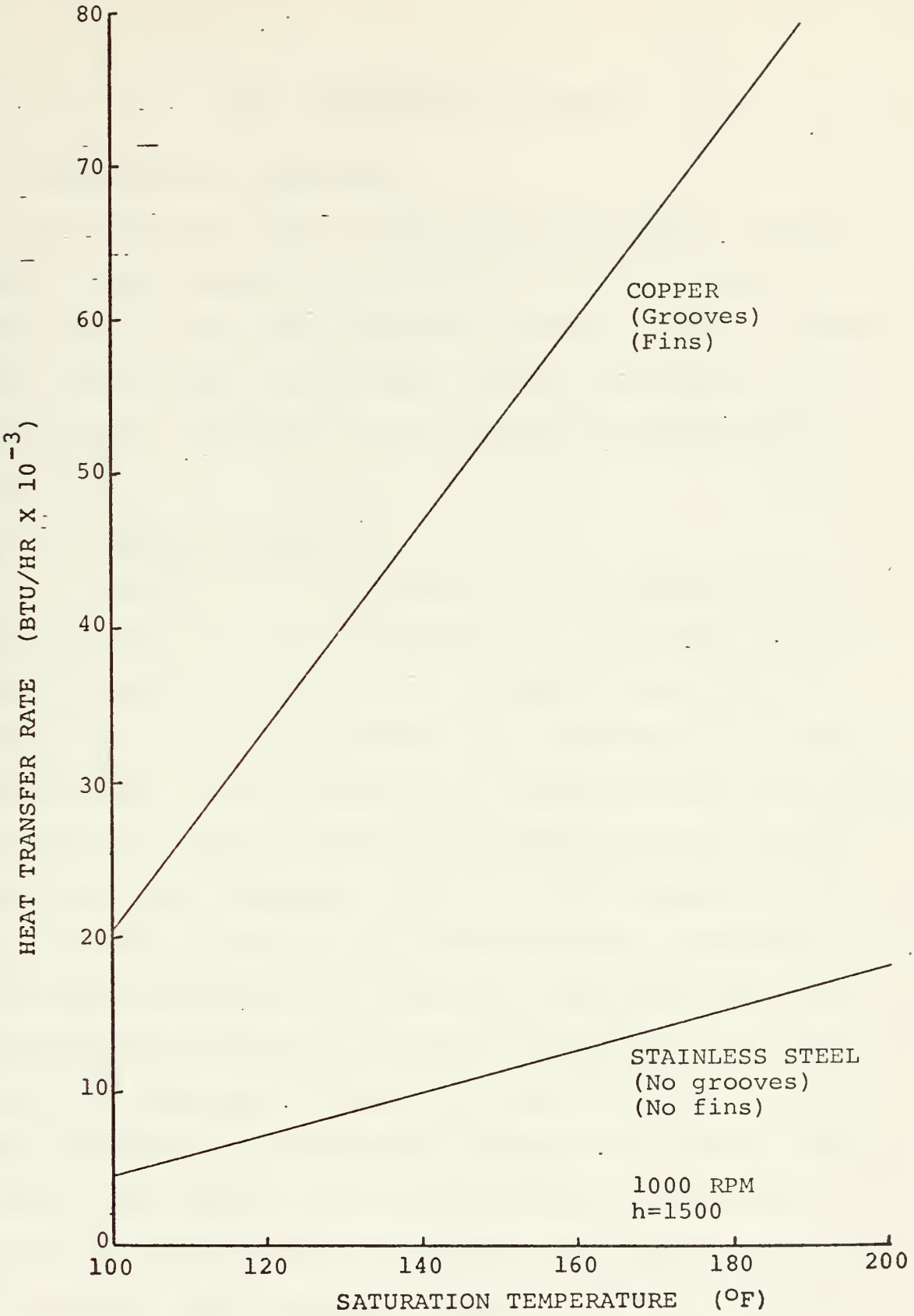

Figure 9 Heat Transfer Rate vs. Saturation Temperature

III. EXPERIMENTAL PROGRAM

A. DESCRIPTION OF EQUIPMENT

The equipment used to support the experimental program was the same equipment used by Newton [5] and Woodard [6]. Some changes were made as described below in order to improve upon data accuracy and increase overall performance of the thermosyphon. Figures 10 and 11 depict the experimental apparatus.

1. Copper Test Section

The use of a test section having a higher thermal conductivity was previously discussed. Copper was chosen as the best material available and a suitable piece of pure oxygen-free copper was purchased for construction of the new thermosyphon. A new condenser and evaporator were constructed. The condenser was machined to the same dimensions as the 1° stainless steel condenser. Length of the evaporator had to be 1/2 inch shorter than its stainless steel counterpart, but all other dimensions were identical. Stainless steel end-pieces were manufactured for the evaporator and the larger end of the condenser in order to reduce the amount of axial heat conduction. The evaporator flanges and inconel heater element were bonded to the copper section in a hydrogen furnace at 1850°F using a 50% copper - 50% gold brazing foil. The condenser and its mating flange were joined using high temperature (1050°F) silver solder. Assembly of the copper evaporator and condenser then followed the guidelines

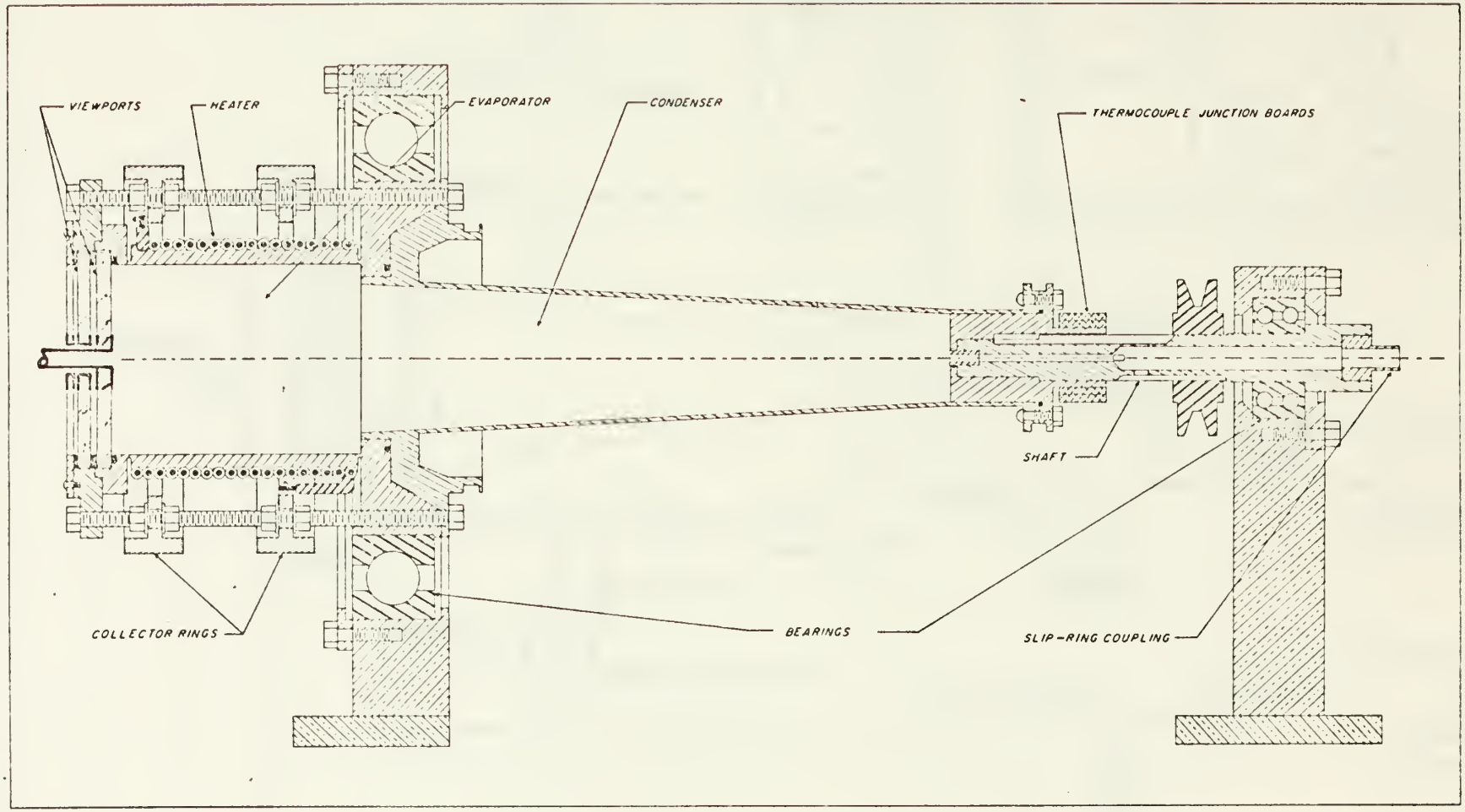

FIGURE 10 CROSS SECTION OF ROTATING HEAT PIPE

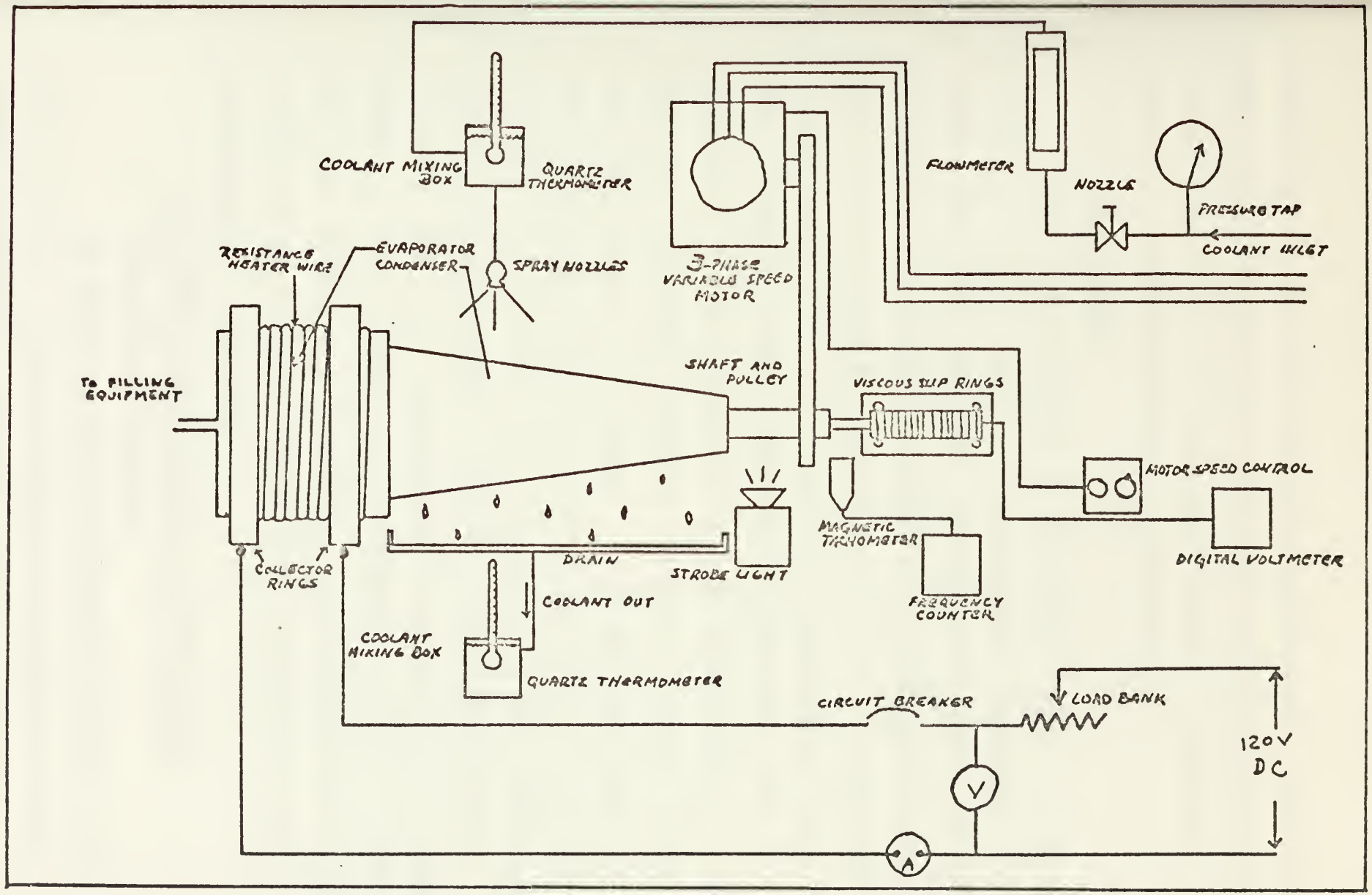

Figure 11 Thermosyphon Equipment Schematic

established by the stainless steel thermosyphon. New bearings and Garlock seals were installed on the new test section to eliminate some of the noise and vibration experienced in rotation of the stainless steel thermosyphon.

2. Power Supply

Power was furnished to the heater coils by a 120 volt DC motor generator having an automatically regulated voltage output. The use of parallel connected resistance load banks in series with the heater element gave stable heater power levels from 0.433 kw to a maximum of 8.0 kw. To meet the higher power levels that an improved thermosyphon design could handle, it became necessary to change the power source. One phase of a three phase 208 volt AC power line was connected across the load banks and heater element. Circuit breakers were set to trip at 150 amperes The same load bank arrangement was used to regulate the heater coil power level through the range of 0.5 kw to 20 kw. Operation of the thermosyphon with the new power source, however, created unacceptable levels of random noise generation in all eight of the thermocouples. Brush adjustments and attempts to ground out the noise were uniformly unsuccessful. Time constraints dictated a return to the DC power supply which continued to prove satisfactory in operation.

3. Instrumentation and Coolant Modifications

a. Thermocouple Location

To obtain a better temperature profile for the condenser wall, six thermocouples were used in an uneven spacing arrangement. These were located at distances of

0.0, 0.5, 1.25, 2.0, 3.0 and 5.3 inches from the flange that mates the evaporator and condenser sections (Figure 10).

b. No Load Heat Generation

Since heat was being generated by the bearing and Garlock seal and transmitted through the condenser flange, it became evident that the coolant was picking up some portion of this. Both copper and stainless steel test sections were run under no load conditions to determine the amount of heat generation received by the coolant.

$$q_{coolant} = \dot{m} C_p \Delta T \qquad (28)$$

where ΔT = temperature difference of coolant

$\dot{m}$ = mass rate of coolant flow

an uncertainty value of $\pm$ 25% was assigned to this data due to the nature of the source and the measurement techniques. Corrections (as shown in Table 2) were then applied to the previously obtained data. Even though the flange area of the copper thermosyphon was insulated with low conductivity silicone rubber during assembly, it did have a greater amount of no load heat generation than the stainless steel thermosyphon. It is felt that the larger number of thermocouple wires strung along the copper condenser imparted this increase in energy to the coolant.

RPM	Q_ℓ-STAINLESS (Btu/hr)	Q_ℓ-COPPER (Btu/hr)
700	236±59	
1000		591±148
1400	394±97	
2100	571±143	866±216
2800	807±201	1162±291

Table 2 No Load Heat Generation for Stainless Steel and Copper Thermosyphons

c. Thermocouple Attachment

The technique for welding surface temperature measuring thermocouples described by ref. 6 was used successfully for the stainless steel condenser. However, this procedure did not work for the copper condenser section. Small grooves, .010 inches deep, were machined in the wall at the desired thermocouple locations. These grooves were then filled with solder. The kapton insulation was removed from the thermocouple wire, exposing about 1/8 inch of the invidual copper and constantan wires. The bare wires were then cleaned and the tips twisted together. This junction was then tinned with the same solder. A small oxygen-acetylene torch applied locally to the inside surface of the condenser would melt the solder at an individual thermocouple location and the tinned junction could easily be placed at the desired spot. A strongly bonded thermocouple junction resulted that would give the average surface temperature between the locations that the wires penetrated the solder surface. The thermocouple wires were then tied down with loops of copper along the length of the condenser.

B. EXPERIMENTAL PROCEDURES

The experimental procedures involve cleaning of the thermosyphon, filling with the working fluid, and operating procedures.

1. Cleaning Procedures

The interior surface of the thermosyphon had to be adequately cleaned to insure proper wetting by the working fluid. If the stainless steel and copper test sections were not cleaned properly, dropwise rather than film condensation would be obtained with water as the working fluid. As explained in Woodard's study [6], the theoretical model was based on film condensation, and dropwise condensation results could not be predicted. Both ethanol and freon 113 were found to have excellent wetting characteristics with stainless steel and no prescribed cleaning procedures were necessary. The cleaning procedure described in ref. 6 was satisfactory for the stainless steel thermosyphon and water. Obtaining film condensation on copper required different cleaning procedures. The method that worked was a modification of a procedure used in preparing copper for electroplating [12]. The following is the appropriate cleaning procedure for the copper thermosyphon:

a. Place the thermosyphon in the vertical position and mount the fill equipment.

b. With end windows and "O" rings removed, fill the thermosyphon with a chlorinated hydrocarbon

degreasing compound such as Trichlorethylene. Scrub the entire surface with a stiff bottle brush. (Avoid prolonged breathing of vapors).

c. Drain and rinse with tap water.

d. Fill the thermosyphon with a mixture of sodium hydroxide solution and 200 ml of ethyl alcohol. Warm the mixture to approximately 180°F. Scrub with a stiff bottle brush.

e. Drain and rinse with tap water.

f. Fill the thermosyphon with a 10-15 percent sulfuric acid solution at room temperature. Scrub with a stiff bottle brush. Do not leave solution in thermosyphon longer than 5 minutes.

g. Drain and rinse with tap water.

h. Rinse three times with distilled water.

i. When ready to fill, prepare the end windows for installation, drain the thermosyphon, install the end windows with the appropriate "O" ring, gasket, and bolt ring. Torque the bolts to 30 lb-in.

j. Immediately connect the fill equipment and start the vacuum pump.

2. Filling Procedures

Evacuation of the thermosyphon and charging with the working fluid was done as described in ref. 6. Pumping time for the vacuum system was increased, however, to allow for complete evaporation of any liquid remaining in the thermosyphon. Longer pumping times (10-20 hours) and use of the

diffusion pump gave vacuums of less than 100 microns pressure. Care was taken to insure the mercury manometer on the filling apparatus was secured after the initial vacuum was drawn. The mercury vaporizes easily and would have contaminated the interior surfaces of the thermosyphon.

3. Operational Procedures

Operating procedures remain basically the same as those described in ref. 6. Prior to applying power to the heater element, the thermosyphon was run at operational speeds to be used and a set of no load heat generation data taken for each RPM.

C. EXPERIMENTAL RESULTS

1. Stainless Steel Condenser

The stainless steel thermosyphon was operated quanitatively four times. De-ionized distilled water was used as the working fluid for two runs; ethyl alcohol, and freon 113 were used for the other two. Limitations on operation of the thermosyphon were the temperature of the heating coil (indicated by a red glow) and the operating pressure in the vapor space. Pressure in the thermosyphon was not allowed to exceed atmospheric pressure by more than 1-2 psi. Such limitations precluded operation at low RPM's with high power levels. As indicated by Figures 12, 13, 14, and 15, water had a higher operating capacity than either ethyl alcohol or freon 113.

Visual observations were made through the end window with a strobe light. In all operating cases, film condensation

appeared to be taking place since the condenser surface was mirror smooth. Only in the water run of 3 May 1972 did a spot of dropwise condensation appear over an insignificantly small portion of the surface.

2. Copper Condenser

Using the new thermosyphon of copper, a data run using water as the working fluid was conducted 8 November 1972. Film condensation was again witnessed over all but a very small portion of the condenser surface.

3. Coolant Flow

During the data run with the copper thermosyphon, an attempt was made at modifying the external heat transfer coefficient. Coolant flow was increased to the maximum possible with the presently installed system. Analysis of the data showed a small but insignificant increase in the heat transfer coefficient from 1500 to 1650 Btu/hr-ft^2-°F.

A different modification was to aim one of the coolant spray nozzles towards the evaporator end of the condenser (hottest end). Data analysis again showed no significant change in the coefficient or heat transfer rate. This change of coolant pattern did, however, flatten the condenser temperature gradient to a small degree as shown in Figure 17.

4. Discussion of Experimental Results

The results obtained while operating both thermosyphons are plotted in Figures 12, 13, 14, 15, and 16 together with solutions of the analytical model for conditions obtained during operation. The two water runs on the stainless steel

condenser establish repeatability since the same cleaning and filling procedures were used both times. Results from these two runs also compare very closely to those achieved by Woodard [6] under similar conditions. In each of the last two cases, a better thermosyphon vacuum than Woodard's runs was achieved prior to filling (less than 100 microns Hg compared to 4.5 mm Hg). The noted difference between the experimental results and the analytical curve was suggested to be a result of the presence of non-condensible gases in Woodard's study. A higher degree of vacuum, however, would lessen the amount of non-condensibles in the thermosyphons and give closer experimental and analytical results. Such was not the case and the difference cannot be readily explained. It may be speculated that a minute quantity of non-condensible gas under high gravity forces would tend to have the same blanketing effect as a greater amount of non-condensible gas.

The alcohol and freon runs, besides having a lesser heat transfer capability than water, had the unique distinction of giving experimental data that exceeded the analytical solution. This trend is also in agreement with the freon results presented by Lee and Mital [2]. An adequate explanation cannot be deduced other than to note that constant magnitude errors for all runs would be more readily apparent under the lower heat loads. The high heat transfer capabilities of water could overshadow errors that become significant for alcohol and freon.

The results for the copper thermosyphon display the same trend as the water-stainless steel runs. Figure 16 shows that the heat transfer for copper was less than stainless steel at low saturation temperature while it was greater than stainless steel at higher saturation temperatures. The results for each still do not differ by any great amount. This was expected since the external heat transfer coefficient and internal condensate film were the controlling thermal resistances. The difference between experimental and theoretical results for the copper test section is much larger than the differences encountered in the stainless steel runs. Analysis of the data has indicated that the thermocouple located 5.3 inches from the evaporator section may have been reading incorrectly. The temperature distribution over the condenser surface was generated from length x=0 to x=5.3 inches using the thermocouple data in a least squares polynomial and then from x=5.3 to x=9 inches the temperature distribution was given a constant value that was equal to the reading of the thermocouple located at 5.3 inches. Such a temperature distribution is illustrated in Figures 17, 18, and 19. An erratic reading for the thermocouple located at x=5.3 inches would therefore give erroneous theoretical results; even accounting for the curvature at the start of the theoretical curve for the copper run (Figure 16). Another reason for the larger difference between experiment and theory may be due to a gradual loss of thermosyphon vacuum (and resultant introduction of non-condensible gases). A vacuum of 100

microns Hg was achieved prior to filling and sealing, and the data run was started seven hours later. Another data run on the succeeding day had to be aborted, however, because the maximum capacity of the thermosyphon was only 3 KW of power. Such a drop in heat transfer capacity (from 8 KW to 3 KW) with time can only be explained by a slow loss of vacuum.

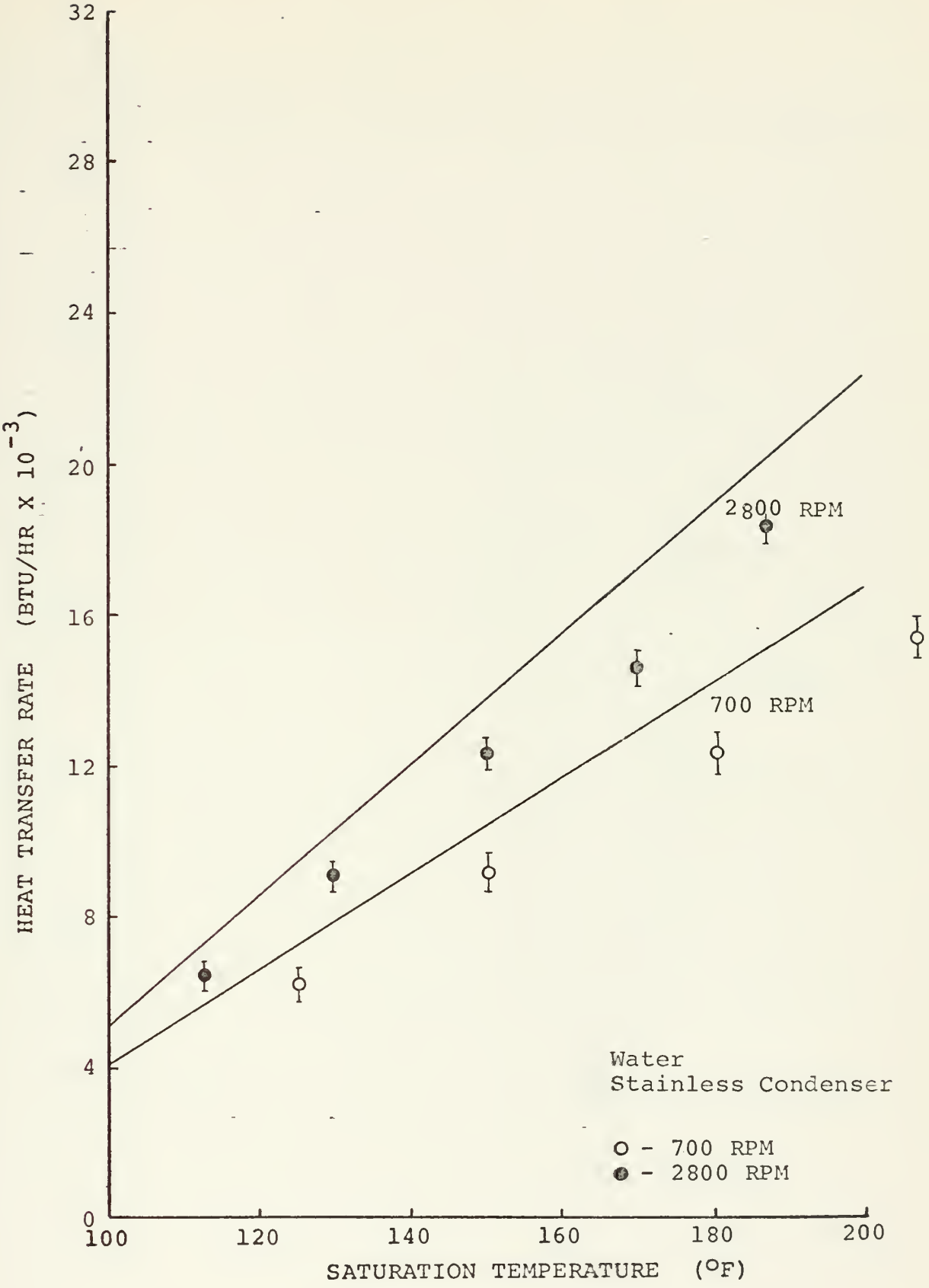

Figure 12 Thermosyphon Heat Transfer Rate vs. Saturation Temperature, 3 May 1972 experimental operation

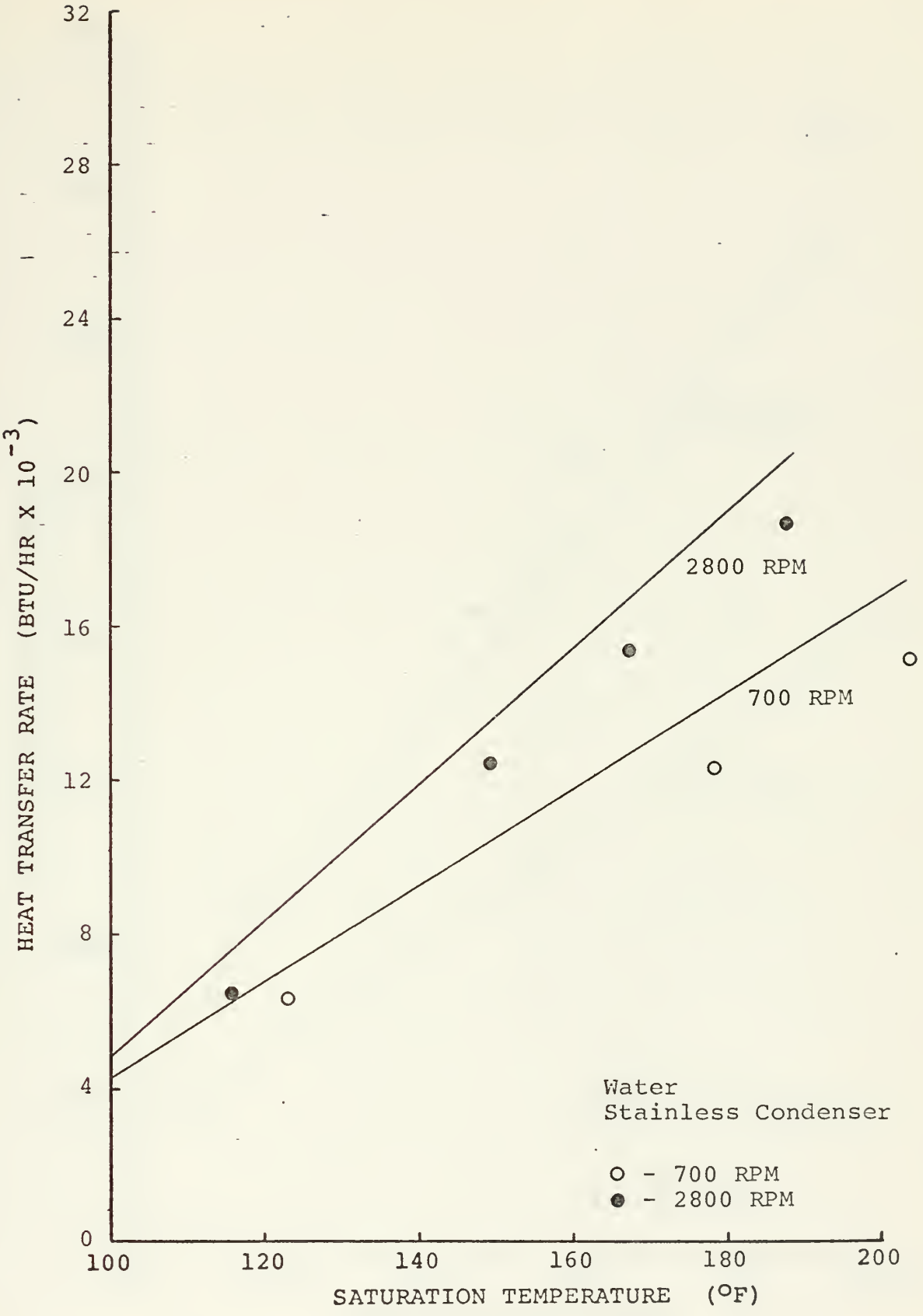

Figure 13 Thermosyphon Heat Transfer Rate vs. Saturation Temperature, 22 May 1972 experimental operation

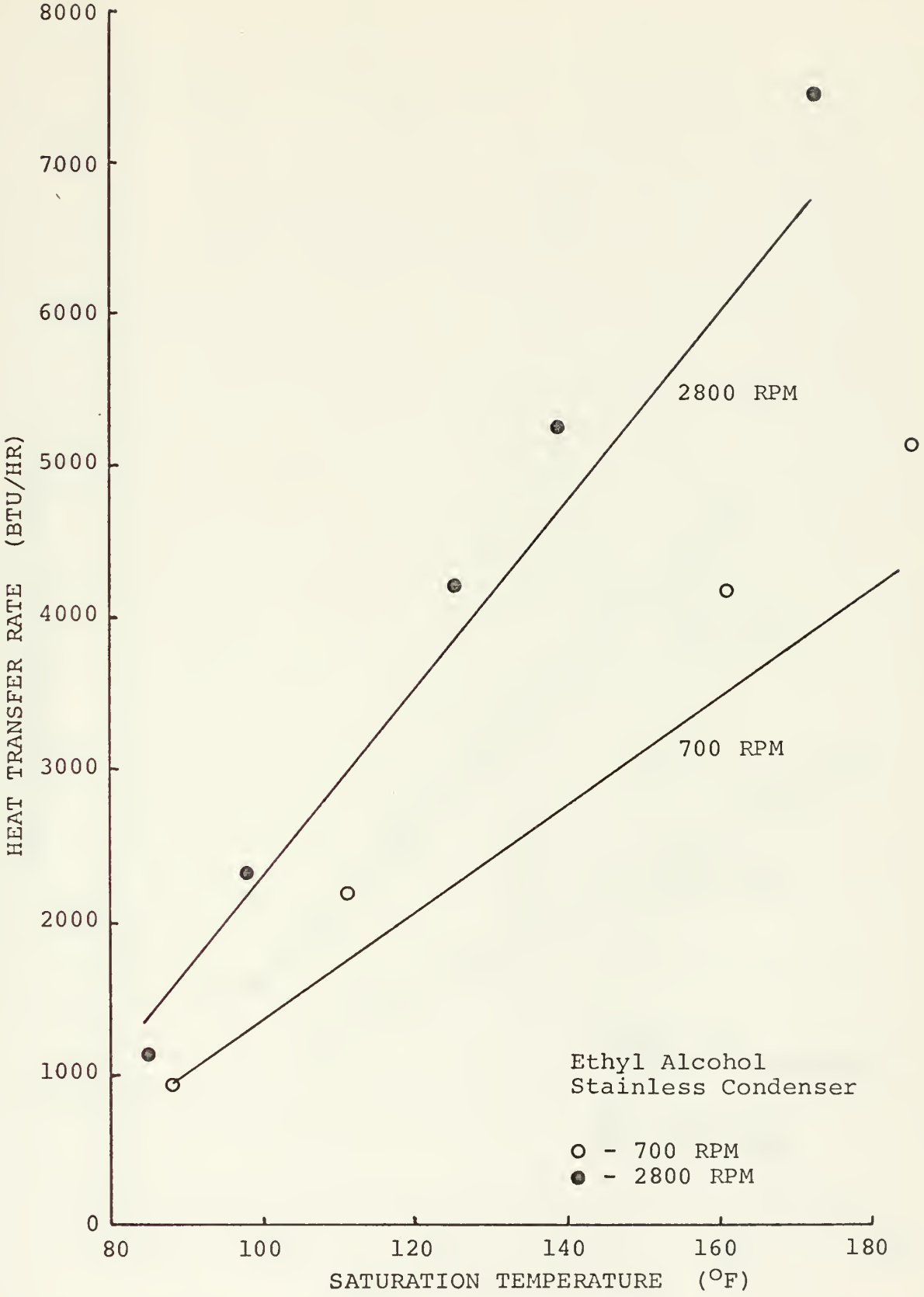

Figure 14 Thermosyphon Heat Transfer Rate vs. Saturation Temperature, 2 June 1972 experimental operation

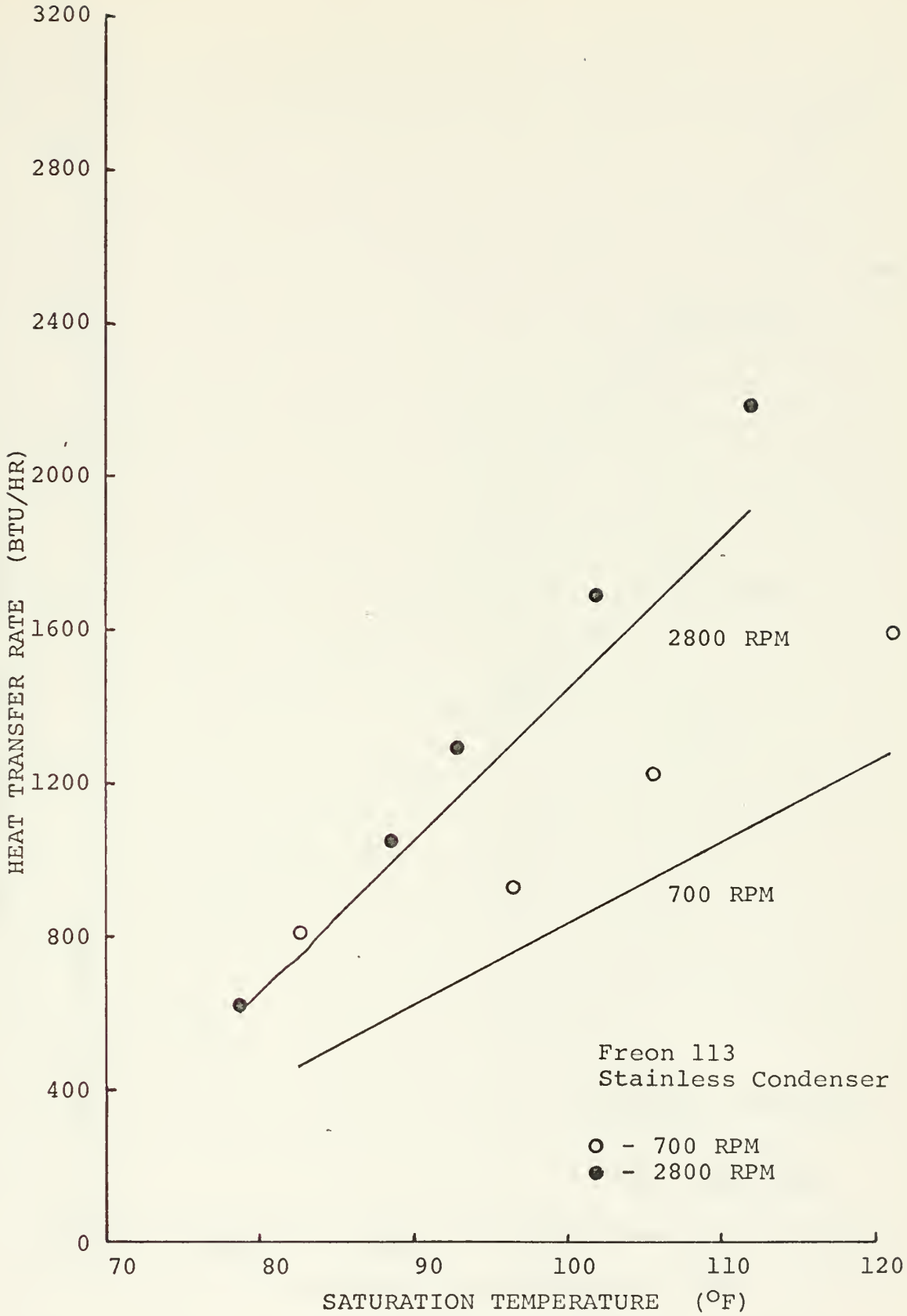

Figure 15 Thermosyphon Heat Transfer Rate vs. Saturation Temperature, 7 June 1972 experimental operation

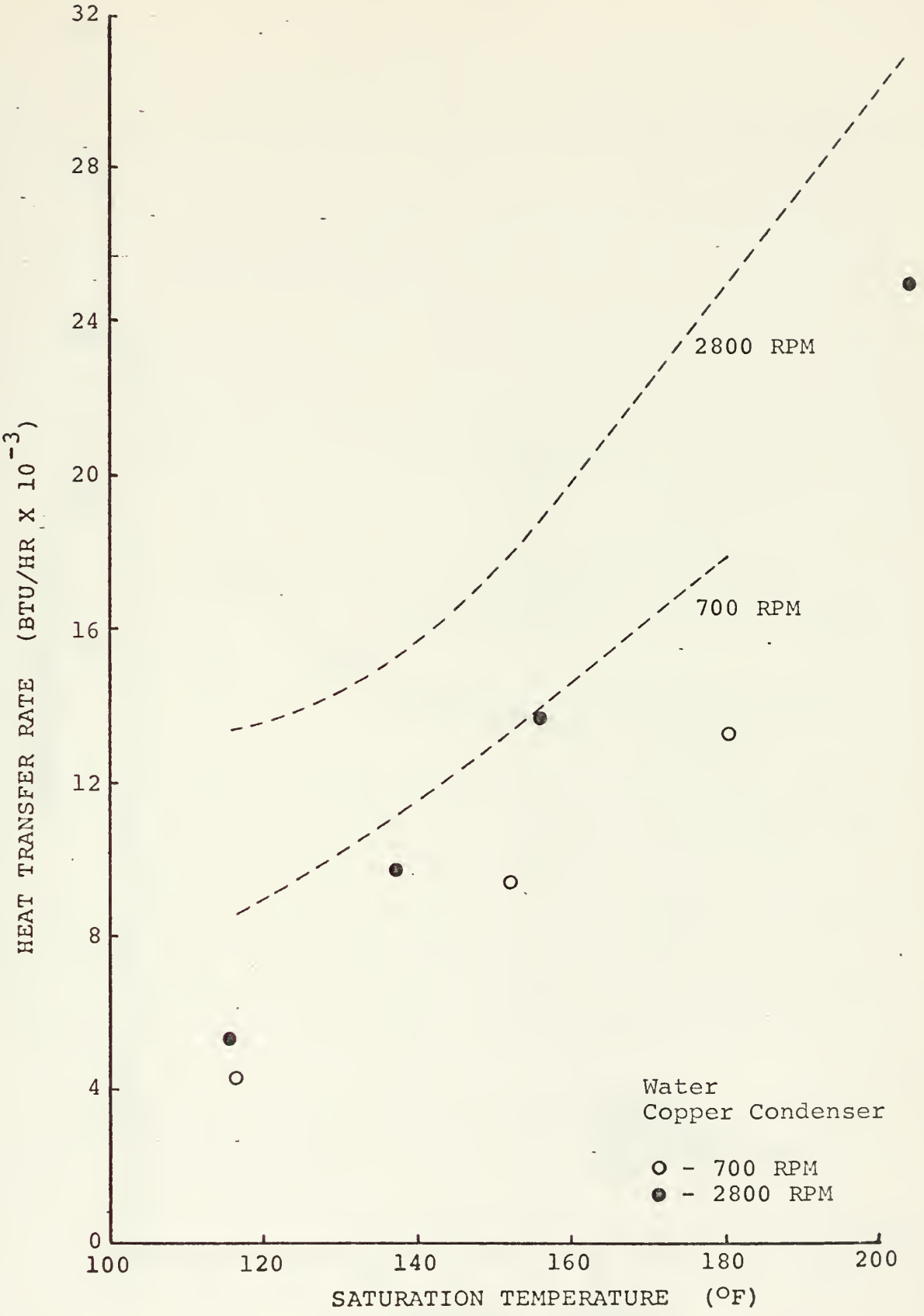

Figure 16 Thermosyphon Heat Transfer Rate vs. Saturation Temperature, 8 November 1972 experimental operation

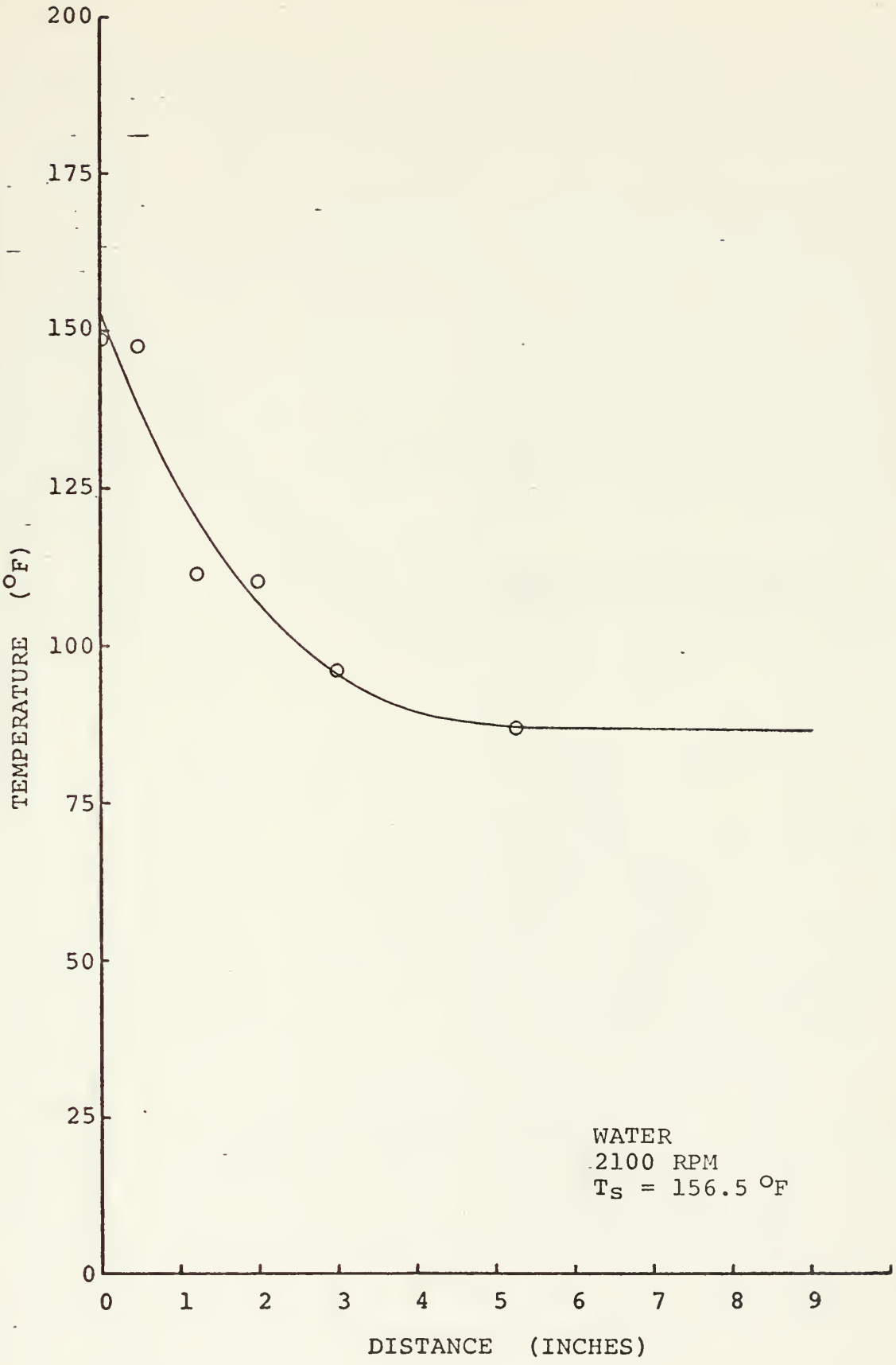

Figure 17 Stainless Steel Condenser Outside Wall Temperature Profile (Normal Spray Cooling)

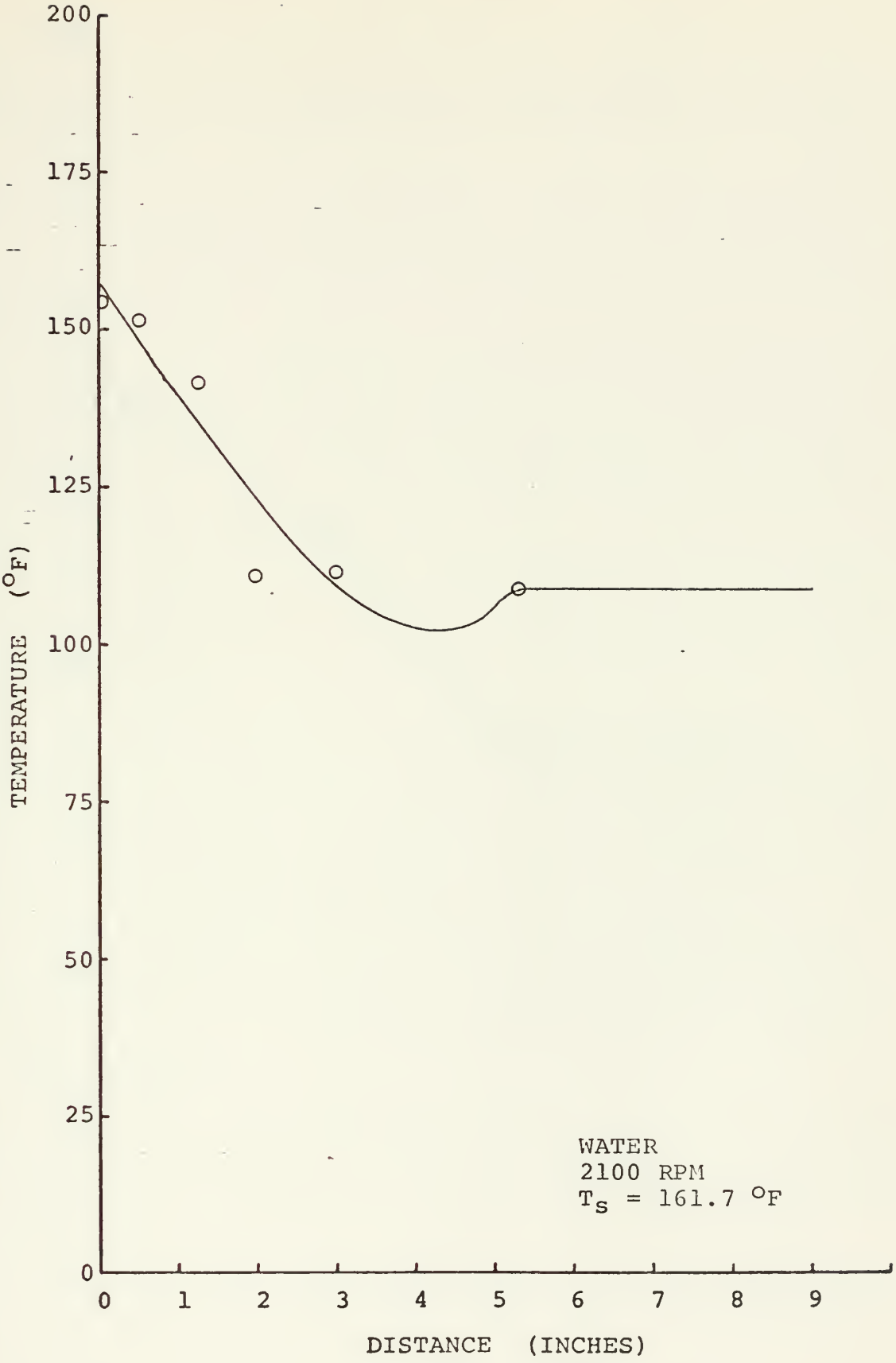

Figure 18 Copper Condenser Outside Wall Temperature Profile (Normal Spray Cooling)

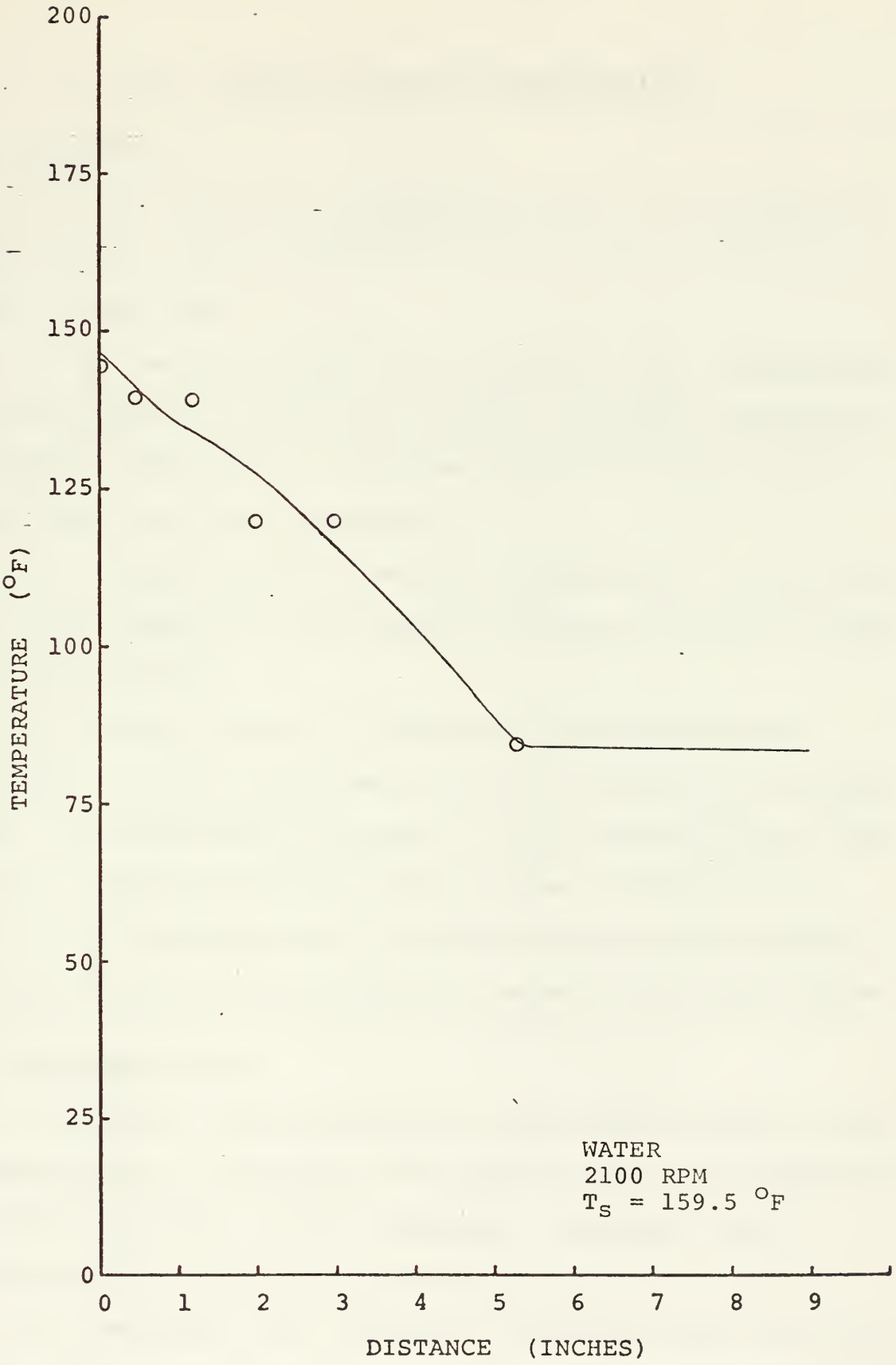

Figure 19 Copper Condenser Outside Wall Temperature Profile (Nozzle inwards)

IV. CONCLUSIONS AND RECOMMENDATIONS

A. CONCLUSIONS

1. The rotating two-phase thermosyphon is an effective heat transfer device capable of transferring very high heat loads at high RPM.

2. The analysis shows that performance of a thermosyphon of the dimensions used in this study is strongly influenced by thermal resistance of condensate film thickness and external heat transfer coefficient.

3. The performance of the same thermosyphon is influenced to a lesser degree by the thermal resistance presented by the wall conductivity.

4. Effective means of minimizing the three thermal resistances of the condenser include the addition of external fins, the longitudinal grooving of the internal surface, and use of a material having a higher thermal conductivity.

5. The performance of the thermosyphon may be degraded by the presence of non-condensible gases in the vapor spaces.

B. RECOMMENDATIONS

1. Conduct a two-dimensional conduction analysis in the condenser wall to determine the actual temperature distribution for the internally grooved condenser. Implement such a solution into the analytical solution.

2. Investigate heat transfer capabilities for internally grooved condenser having other than triangular profiles.

3. Improve the external cooling method by addition of fins or re-design of the cooling system.

4. Conduct a systematic study of the effects of non-condensible gases on thermosyphon performance. Devise a method to determine the concentration of non-condensible gases in the system.

5. Improve the condenser surface temperature measurement of the copper condenser by addition of more thermocouples and implementing better calibration techniques for the thermocouples.

APPENDIX A

CALIBRATION

1. Calibration of the Rotameter. The cooling water rotameter was calibrated by using a Toledo scale and stopwatch to measure the mass rate of flow of coolant flowing into a large receptacle placed on the scale. As coolant flowed into the container, an arbitrary point on the scale was established for starting the stopwatch. When the weight of water had increased by 40 pounds, the timer was stopped and the time interval recorded. This procedure was repeated three times at each flow rate and the average time interval was calculated. Data was taken for 10, 20, 25, 30, 35, and 40% full rotameter scale flow rates. To insure that the flow duplicated experimental conditions, the coolant was allowed to take its normal flow path through the thermosyphon cooling box. The drain hose from the cooling box then emptied directly into the weight tank. (The scale and tank were placed in the gutter to maintain proper flow in the drain hose.) Data was plotted (Figure 20) and a straight line drawn through the points. The equation for that line was found to agree within 1% of the flow rate measured directly by the rotameter scale reading. A correction factor was calculated and the actual flow rate was determined from the following equation

$$\dot{m} = 75 + 34(\%) \qquad \text{lbm/hr} \qquad (29)$$

where % is the rotameter setting.

2. Calibration of Thermocouples. Since the condenser surface thermocouples were manufactured in place, ordinary means of calibration were not available. Instead, the thermosyphon was thermally insulated to the most practical degree and a source of steam introduced into the interior of the condenser. After the condenser had warmed up, another source of steam was blown directly across the thermocouple to be calibrated. In this manner, it was determined that the surface thermocouples for the stainless steel thermosyphon deviated less than $\pm$ 2.0°F from the steam point. A larger and unacceptable deviation occurred for the thermocouples on the copper condenser. It was hypothesized that this larger difference resulted from the high thermal conductivity of copper and inadequate insulation. Calibration for the copper test section was then accomplished by measuring the temperature of cooling water by the thermocouples and previously calibrated quartz thermometers. Agreement was found to be within $\pm$ 2.0°F.

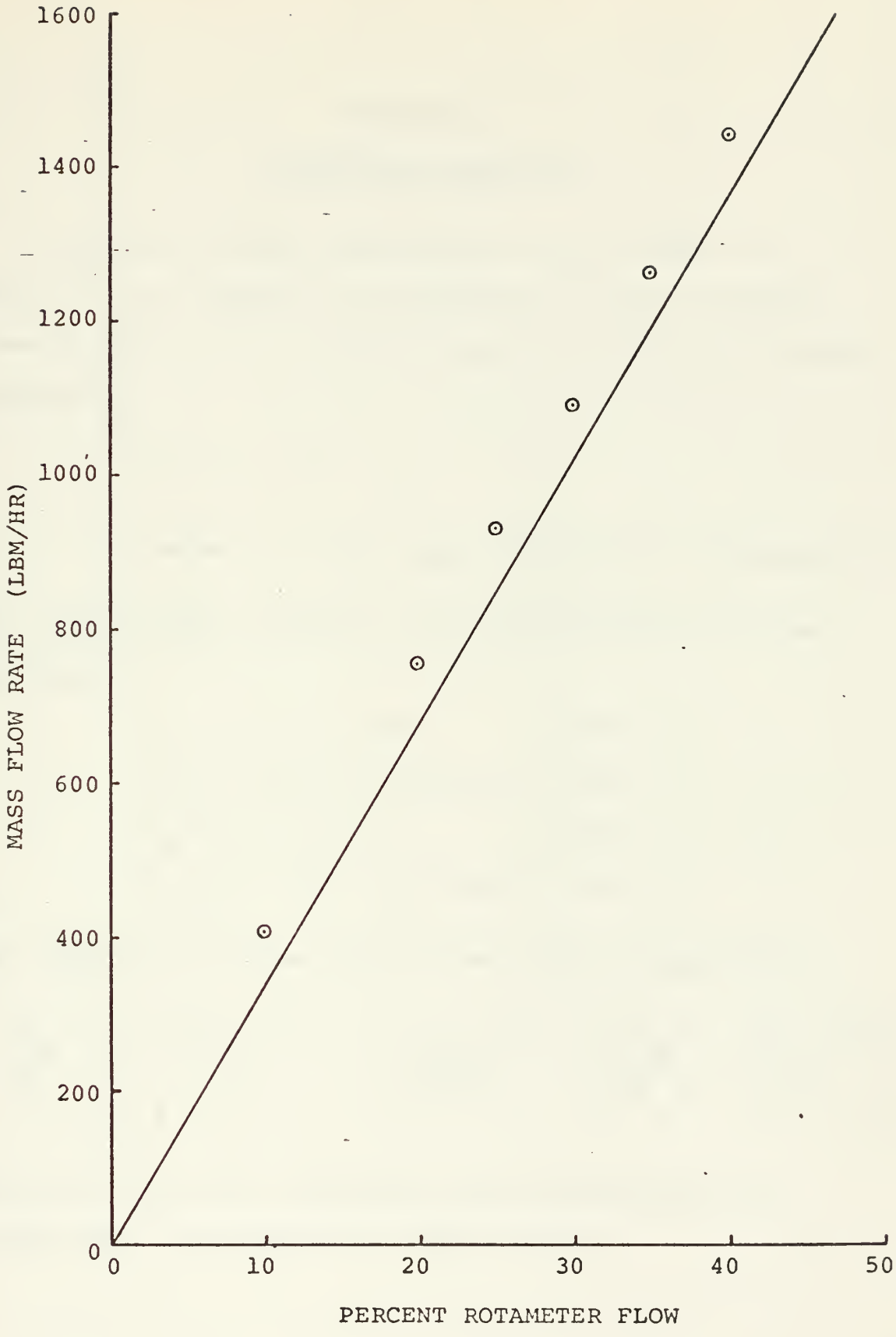

Figure 20 Calibration of 6.8 GPM Rotameter

APPENDIX B

UNCERTAINTY ANALYSIS

Uncertainty in the experimental results (shown in Figure 12) was computed in accordance with the procedure given by Holman [13]. The heat transfer of the thermosyphon is given by

$$Q = \dot{m}\, C_p\, \Delta T - Q_\ell$$

where $Q_\ell = \dot{m}\, C_p\, \Delta T_\ell$ (heat from no load generation)

The uncertainties in each of the above quantities may be expressed as

$W_{\dot{m}} = \pm$ 17.0 lbm/hr (20 to 1)

$W_{C_p} = \pm$ 00.001 Btu/lbm-°F (20 to 1)

$W_{\Delta T} = \pm$ 0.1 °C (20 to 1)

$W_{Q_\ell} = \pm$ 0.25 Q_ℓ Btu/hr (20 to 1)

The uncertainty in heat transfer may then be expressed as

$$\frac{W_Q}{Q} = \left[\left(\frac{W_{\dot{m}}}{\dot{m}} \right)^2 + \left(\frac{W_{\Delta T}}{\Delta T} \right)^2 + \left(\frac{W_{Q_\ell}}{Q} \right)^2 + \left(\frac{W_{C_p}}{C_p} \right)^2 \right]^{\frac{1}{2}}$$

Using the 3 May 1972, stainless steel thermosyphon run at 2800 RPM, the uncertainty limits become

T_s	Q	UNCERTAINTY	
94.0	3431	±289	6.8%
112.9	6374	±303	4.2%
130.0	9180	±322	3.2%
150.5	12338	±348	2.6%
169.4	15576	±380	2.3%
187.1	18401	±411	2.1%

Uncertainty in no load heat generation proved to be the dominating factor. As shown above, its effect is most noticeable at low heat transfer rates.

APPENDIX C

TABULATED DATA

Water

Stainless Steel Condenser

Half Cone Angle = 1°

RPM / T_s	1000	2000	3000
H=1000			
100.0	3994.5	4558.8	4845.9
120.0	6446.6	7421.0	7924.0
140.0	8877.8	10270.8	10994.0
160.0	11310.4	13122.8	14066.9
180.0	13741.9	15972.0	17137.0
200.0	16162.3	18808.3	20195.1
H=1500			
100.0	4532.9	5303.6	5714.5
120.0	7266.0	8582.2	9295.1
140.0	9969.6	11841.2	12861.4
160.0	12675.1	15102.6	16431.0
180.0	15381.0	18361.4	19997.6
200.0	18075.8	21605.2	23548.5
H=5000			
100.0	5539.9	6807.5	7548.8
120.0	8755.2	10869.3	12127.1
140.0	11923.7	14890.5	16669.3
160.0	15093.0	18912.3	21213.2
180.0	18266.6	22934.3	25755.2
200.0	21432.4	26939.9	30276.9

Water

Copper Condenser

Half Cone Angle = 1°

RPM / T_s	1000	2000	3000
H=1000			
100.0	4971.0	5938.7	6474.7
120.0	7917.3	9550.4	10470.0
140.0	10824.6	13130.6	14437.4
160.0	13731.3	16708.2	18401.6
180.0	16637.8	20279.8	22356.7
200.0	19531.7	23870.8	26287.7
H=1500			
100.0	5780.7	7188.0	8030.3
120.0	9099.8	11429.8	12846.4
140.0	12365.9	15619.8	17612.5
160.0	15630.4	19805.8	22373.7
180.0	18898.7	23989.0	27128.0
200.0	22158.7	28152.9	31856.2
H=5000			
100.0	7339.2	9898.7	11688.4
120.0	11279.7	15316.0	18162.5
140.0	15128.3	20612.3	24499.5
160.0	18967.4	25890.7	30814.7
180.0	22816.5	31175.1	37133.4
200.0	26669.7	36456.8	43443.2

Water

Internally Grooved Stainless Steel Condenser

Half Cone Angle = 1°

Fin Half Angle	H_{T_s}	RPM=1000		
		1000	1500	5000
10°	100	4253	5295	8251
	150	11124	13811	21451
	200	17991	22322	34616
20°	100	4232	5256	8115
	150	11063	13694	21017
	200	17889	22124	33865
30°	100	4226	5232	7990
	150	11040	13617	20628
	200	17848	21989	33202
40°	100	4213	5194	7827
	150	10996	13502	20159
	200	17773	21797	32425
		RPM=3000		
10°	100	4580	5763	9096
	150	12060	15125	23712
	200	19546	24495	38332
20°	100	4564	5734	9007
	150	12014	15045	23455
	200	19473	24364	37902
30°	100	4563	5723	8926
	150	12012	15009	23221
	200	19469	24305	37510
40°	100	4557	5698	8802
	150	11994	14939	22871
	200	19438	24188	36930

Water

Internally Grooved Copper Condenser

Half Cone Angle = 1°

RPM=1000

Fin Half Angle	H / T_s	1000	1500	5000
10°	100	5720	7978	20983
	150	14914	20764	53680
	200	24072	33488	85619
20°	100	5692	7899	19699
	150	14822	20487	49375
	200	23910	32996	78218
30°	100	5697	7866	18794
	150	14815	20342	46893
	200	23888	32729	74549
40°	100	5709	7843	18142
	150	14825	20234	45634
	200	23894	32532	73243

RPM=3000

10°	100	6193	8694	22896
	150	16266	22698	59634
	200	26223	36648	96156
20°	100	6180	8660	22346
	150	16187	22588	57783
	200	26157	36461	92912
30°	100	6303	8675	21927
	150	16240	22608	56342
	200	26240	36482	90394
40°	100	6234	8701	21530
	150	16316	22654	55042
	200	26360	36544	88172

TABULATED EXPERIMENTAL DATA

8 November 1972

Water

Copper Condenser

Half Cone Angle = 1°

Standard Cooling Water Nozzle Arrangement

RPM	T_s	Q-EXPERIMENTAL	Q-THEORY
1000	116.5	4323	8599
	151.9	9432	13428
	179.7	13186	17860
2100	115.8	4520	12433
	141.0	9472	14048
	161.7	13284	18614
	214.3	24819	31344
2800	115.5	5266	13442
	136.9	9747	14432
	155.4	13736	18744
	203.8	25094	31007

3 May 1972

Water

Stainless Steel Condenser

Half Cone Angle = 1°

Standard Cooling Water Nozzle Arrangement

RPM	T_s	Q-EXPERIMENTAL	Q-THEORY
700	95.1	3394	3364
	125.4	6199	7503
	150.5	9142	10661
	180.5	12321	14604
	207.0	15342	17660
	230.1	18128	20304
1400	95.7	3295	4065
	117.5	6296	7468
	138.9	9298	10744
	164.0	12359	14404
	186.9	15734	17875
	206.0	18304	20695
2100	95.3	3373	4301
	115.1	6355	7681
	132.4	9278	10405
	156.5	12300	14381
	174.6	15714	17533
	194.5	18303	20375
2800	94.0	3431	4235
	112.9	6374	6576
	130.0	9180	10589
	150.5	12338	14196
	169.4	15576	17464
	187.1	18401	20108

22 May 1972

- Water

Stainless Steel Condenser

Half Cone Angle = 1°

Standard Cooling Water Nozzle Arrangement

RPM	T_s	Q-EXPERIMENTAL	Q-THEORY
700	96.6	3448	3824
	123.0	6309	7198
	177.9	12344	14095
	203.5	15185	17248
1400	94.2	3447	3958
	116.7	6327	7229
	162.8	12401	14084
	184.0	15282	17201
	206.0	18671	20566
2100	94.0	3485	4177
	114.0	6463	7381
	155.1	12420	14089
	175.1	15281	17317
	194.5	18651	20637
2800	92.9	3602	4128
	115.5	6423	7689
	149.2	12458	13909
	166.9	15358	16978
	187.5	18650	20436

2 June 1972

Ethyl Alcohol

Stainless Steel Condenser

Half Cone Angle = 1°

Standard Cooling Water Nozzle Arrangement

RPM	T_s	Q-EXPERIMENTAL	Q-THEORY
700	88.0	925	954
	111.2	2185	1863
	160.9	4173	3558
	186.2	5118	4370
1400	87.5	984	1175
	104.6	2244	2063
	142.4	4232	3804
	162.0	5177	4646
	205.9	7303	6473
2100	86.6	1083	1282
	101.3	2264	2199
	132.7	4291	3928
	149.3	5275	4777
	188.2	7421	6748
2800	85.3	1122	1331
	97.9	2323	2214
	125.5	4331	3934
	138.9	5256	4717
	172.9	7460	6708

7 June 1972

Freon 113

Stainless Steel Condenser

Half Cone Angle = 1°

Standard Cooling Water Nozzle Arrangement

RPM	T_s	Q-EXPERIMENTAL	Q-THEORY
700	82.7	807	470
	96.6	925	781
	105.6	1221	969
	121.6	1595	1278
1400	81.0	610	560
	93.4	984	929
	99.8	1259	1105
	112.0	1633	1439
	125.5	2086	1786
2100	80.1	630	602
	90.8	1023	984
	96.2	1279	1171
	107.2	1673	1537
	117.8	2145	1864
2800	78.5	610	600
	88.5	1043	1009
	92.7	1299	1180
	102.1	1693	1549
	111.8	2185	1898

BIBLIOGRAPHY

1. Gray, V. H., The Rotating Heat Pipe - A Wickless, Hollow Shaft for Transferring High Heat Fluxes, paper presented at Eleventh National Heat Transfer Conference, Minneapolis, Minnesota, August 3-6, 1969.

2. Lee, Y., and Mital, U., "A Two-Phase Closed Thermosyphon," International Journal of Heat and Mass Transfer, Vol. 15, No. 9, pp. 1695-1707, September 1972.

3. Ballback, L. J., The Operation of a Rotating Wickless Heat Pipe, M.S. Thesis, Naval Postgraduate School Monterey, California, December 1969.

4. Daley, T. J., The Experimental Design and Operation of a Wickless Heat Pipe, M.S. Thesis, Naval Postgraduate School, Monterey, California, June 1970.

5. Newton, W. H., Jr., Performance Characteristics of Rotating, Non-Capillary Heat Pipes, M.S. Thesis, Naval Postgraduate School, Monterey, California, June 1971.

6. Woodard, J. S., The Operation of Rotating Non-Capillary Heat Pipes, M.S. Thesis, Naval Postgraduate School, Monterey, California, March 1972.

7. Holman, J. P., Heat Transfer, 2d. Ed., pp. 33-41, McGraw-Hill, 1963.

8. Moreno, J., Condensation of Steam at Sub-Atmospheric Pressure on a Vertical, Flat Plate, M.S. Thesis, Naval Postgraduate School, Monterey, California, December 1972.

9. Gregorig, R., "Hautkondensation au feingawellten Oberflachen bei Berucksichtigung der Oberflachen-spannungen," Zeitschrift fur angewandte Mathematik und Physik, Vol. V., pp. 36-49, 1954.

10. Lustenader, E. L., Richter, R., and Neugebauer, F. J., "The Use of Thin Films for Increasing Evaporation and Condensation Rates in Process Equipment," Journal of Heat Transfer, Vol. 81, Series C, No. 4, pp. 297-307, November 1959.

11. Hewitt, G. F., Lacey, P. M. C., and Nicholls, B., Transitions in Film Flow in a Vertical Tube, paper presented at Symposium on Two Phase Flow, University of Exeter, June 21-23, 1965.

12. Smithells, C. J., Metals Reference Book, 3rd Ed., Vol. 2, p. 1030, Buttersworth, 1962.

13. Holman, J. P., Experimental Methods for Engineers, 1st Ed., pp. 37-39, McGraw-Hill, 1966.

INITIAL DISTRIBUTION LIST

		No. Copies
1.	Defense Documentation Center Cameron Station Alexandria, Virginia 22314	2
2.	Library, Code 0212 Naval Postgraduate School Monterey, California 93940	2
3.	Professor P. J. Marto, Code 59Mx Department of Mechanical Engineering Naval Postgraduate School Monterey, California 93940	2
4.	Department of Mechanical Engineering, Code 59 Naval Postgraduate School Monterey, California 93940	1
5.	Lieutenant Commander Carl E. Schafer, II 11301 Upper Huntington Road Fort Wayne, Indiana 46804	1

UNCLASSIFIED
Security Classification

DOCUMENT CONTROL DATA - R & D

(Security classification of title, body of abstract and indexing annotation must be entered when the overall report is classified)

ORIGINATING ACTIVITY (Corporate author)

Naval Postgraduate School
Monterey, California 93940

2a. REPORT SECURITY CLASSIFICATION

Unclassified

2b. GROUP

REPORT TITLE

Augmenting the Heat Transfer Performance of Rotating Two-Phase Thermosyphons

DESCRIPTIVE NOTES (Type of report and inclusive dates)

Mechanical Engineer's Thesis; December 1972

AUTHOR(S) (First name, middle initial, last name)

Carl Edward Schafer II

REPORT DATE	7a. TOTAL NO. OF PAGES	7b. NO. OF REFS
December 1972	81	13

a. CONTRACT OR GRANT NO.	9a. ORIGINATOR'S REPORT NUMBER(S)
b. PROJECT NO.	
c.	9b. OTHER REPORT NO(S) (Any other numbers that may be assigned this report)
d.	

10 DISTRIBUTION STATEMENT

Approved for public release; distribution unlimited.

11. SUPPLEMENTARY NOTES	12. SPONSORING MILITARY ACTIVITY
	Naval Postgraduate School Monterey, California 93940

13. ABSTRACT

A Nusselt-type analysis was performed for laminar film condensation on the inside of a truncated rotating cone. Studies of this model revealed that the heat transfer capacity of the rotating thermosyphon was controlled by three thermal resistances; the condensate film thickness, condenser wall resistance, and the external heat transfer coefficient. A parametric study of the solution was performed for various values of these resistances and methods for reducing them were investigated.

A stainless steel thermosyphon was tested using various working fluids. A copper thermosyphon was constructed and tested using water. Different power levels and speeds of rotation were investigated.

Longitudinal grooving was studied as a means of reducing the heat transfer resistance of the internal condenser surface. An analytical model was developed for a triangular groove profile and a parametric analysis performed to show effects on heat transfer capabilities.

DD FORM 1 NOV 68 1473 (PAGE 1)

S/N 0101-807-6811

UNCLASSIFIED
Security Classification

A-31408

14 KEY WORDS	LINK A		LINK B		LINK C	
	ROLE	WT	ROLE	WT	ROLE	WT
Rotating thermosyphon						
Film condensation						
Heat pipe						

29 JUN 76
6 FEB 80
24 JUN 82

23990
26219
28590

141745

Thesis
S2465
c.1

Schafer
Augmenting the heat transfer performance of rotating two-phase thermosyphons.